Scientific Reports

https://doi.org/10.1038/s41598-026-57124-x

Article in Press

Stabilization and solidification of iron ore tailings using alkali-activated geopolymer

Received: 30 March 2026

Accepted: 4 June 2026

Published online: 08 June 2026

Cite this article as: Ghorbanipour A., Hamidi A. & Fini E. Stabilization and solidification of iron ore tailings using alkali-activated geopolymer. *Sci Rep* (2026). https://doi.org/10.1038/s41598-026-57124-x

Arash Ghorbanipour, Amir Hamidi & Elham Fini

Stabilization and Solidification of Iron Ore Tailings Using Alkali-Activated Geopolymer

Arash Ghorbanipour[a], Amir Hamidi[b], Elham Fini[c]

[a]Graduate student, Department of Civil Engineering, School of Engineering, Kharazmi University, Tehran, Iran, arash.ghorbanipour@khu.ac.ir

[b,*]Professor, Department of Civil Engineering, School of Engineering, Kharazmi University, Tehran, Iran, hamidi@khu.ac.ir, ORCID 0000-0002-1662-7516 (Corresponding author)

[c]Associate Professor, School of Sustainable Engineering and the Built Environment, Arizona State University, 660 S. College Avenue, Tempe, AZ, 85287-3005, USA, efini@asu.edu, ORCID 0000-0002-3658-0006

[*]**Corresponding author**

Email: (Amir Hamidi) hamidi@khu.ac.ir

Stabilization and Solidification of Iron Ore Tailings Using Alkali-Activated Geopolymer

Abstract

Iron ore tailings (IOT) exhibit weak mechanical properties and pose environmental concerns, limiting their direct application in geotechnical engineering. This study demonstrates that alkali activation with ground granulated blast furnace slag (GGBFS) enables simultaneous enhancement

of mechanical performance, significant reduction in heavy metal mobility, and lower environmental impacts. Specifically, up to 95% decrease in heavy metal leaching and approximately 35% reduction in environmental impacts were achieved. IOT was activated using sodium hydroxide (NaOH) solutions ranging from 0 to 5 M in combination with GGBFS at replacement levels of 0–9 wt%. Specimens were prepared at optimum moisture content obtained from standard compaction tests and cured for 7, 14, and 28 days. The mechanical, environmental, and microstructural characteristics were evaluated through UU triaxial compression test, one-dimensional consolidation test, scanning electron microscopy with energy-dispersive X-ray spectroscopy (SEM–EDS), toxicity characteristic leaching procedure (TCLP), and life cycle assessment (LCA). The results indicate that alkali activation considerably improves the undrained shear strength of IOT, while GGBFS addition further enhances this improvement. Under a confining pressure of 200 kPa and 5 M NaOH, increasing slag content from 0% to 9% increased shear strength from 1,265 to 5,824 kPa. This behavior was associated with intensified geopolymerization reactions and the formation of a denser microstructure, resulting in nearly doubled cohesion and an approximately 20% increase in internal friction angle compared with untreated tailings. A LCA revealed that using geopolymer-based tailings could lower the global warming potential and energy demand by approximately 35% compared to Portland cement. Beyond the reductions in energy use and CO_2 emissions, the stabilization method also dramatically

suppressed heavy metal mobility, up to a 95% reduction in certain specimens. Overall, the findings confirm the potential of alkali-activated IOT as a sustainable and high-performance material for geotechnical applications.

Keywords: iron ore tailings; sodium hydroxide; ground granulated blast furnace slag; shear strength; life cycle assessment; leaching

Introduction

Mining and construction activities serve as fundamental drivers of economic growth and infrastructure development; however, their rapid expansion has been accompanied by severe environmental challenges. Among these, the generation and long-term accumulation of mine tailings has emerged as a particularly pressing global concern [1, 2]. Worldwide estimates indicate that more than 20 billion tons of tailings are produced annually [3, 4]. In Iran, large IOT operations, such as Golgohar and Chadormalu, alone contribute approximately 15–20 million tons of tailings each year [5, 6]. These materials, typically enriched in SiO_2, Fe_2O_3, MgO, and CaO, exhibit fine textures and clay-bearing phases, which result in high compressibility and low shear strength [7]. Consequently, beyond their environmental risks, they exhibit poor geotechnical performance, which limits their direct use in civil and geotechnical applications [8]. While chemical stabilization strategies, such as adding alkaline agents, lime, or cement have been explored to address these deficiencies, concerns regarding sustainability and carbon emissions persist, challenging the viability of conventional approaches.

At the same time, the cement industry, which produces the second most widely consumed material after water, remains one of the most significant global contributors to CO_2 emissions. Moreover, the annual production of Portland cement continues to grow at a rate of nearly 9% per year [9], and its global output of roughly 4 billion tons results in the release of 800–900 kg of CO2 per ton of product. This results in emissions accounting for about 7–8% of global anthropogenic greenhouse gas emissions [10, 11]. The industry's heavy dependence on non-renewable natural resources and its inherently energy-intensive manufacturing process further exacerbates long-term sustainability concerns. As a result, identifying low-carbon and environmentally compatible alternatives to ordinary Portland cement (OPC) has become a key global research priority [12], and efforts to develop efficient, low-carbon stabilization methods for problematic geomaterials have intensified.

Within this broader context, geopolymers have emerged as promising and environmentally compatible binders capable of addressing both mechanical and sustainability challenges [13]. Calcium-rich additives such as GGBFS accelerate reaction kinetics and enhance both early-age strength and long-term durability in alkali-activated systems [14, 15].

The geopolymerization process is governed by the mineralogical composition of IOT and its interaction with the NaOH–GGBFS system. Under alkaline conditions, dissolution of aluminosilicate phases releases reactive species ($Si(OH)_4$ and $Al(OH)_4^-$), which contribute to the formation of sodium alumino

silicate hydrate (N–A–S–H) gel networks. The addition of GGBFS supplies calcium ions that promote the development of calcium alumino silicate hydrate (C–A–S–H) gels, resulting in a denser microstructure and stronger interparticle bonding [16]. These mechanisms directly control the shear strength and compressibility behavior of the treated IOT.

Geopolymers also provide notable environmental advantages. The LCA studies report CO_2 emissions 40–80% lower than those of OPC [17]. Although the synthesis of alkaline activators such as NaOH and Na_2SiO_3 is energy-intensive and partially offsets these benefits, comprehensive LCA evaluations consistently affirm the overall superiority of geopolymer systems relative to OPC [16, 18, 19]. Beyond reducing carbon emissions, geopolymers exhibit excellent immobilization capacity for heavy metals, significantly restricting the leaching of toxic elements such as Pb, Zn, Cu, Ni, and Co [20]. This makes them particularly suitable for the stabilization and solidification of contaminated mine tailings, where long-term leach resistance is crucial [21].

Despite the recognized potential of geopolymer-stabilized tailings, most existing studies focus primarily on compressive strength, with limited consideration of shear strength and compressibility relevant to geotechnical applications [22]. The combined use of triaxial and consolidation testing together with standardized environmental assessments such as TCLP and LCA remains limited for IOT, and the linkage between microstructural

evolution and geotechnical behavior under varying activation conditions is not yet well established.

Unlike previous studies that address these aspects separately, this work establishes direct links between strength development, compressibility, microstructural evolution, and environmental performance. A summary of relevant studies is provided in Table 1 to highlight variations in materials, activators, and testing approaches and to position the scope of the present work.

Table 1. Summary of previous studies on geopolymers, including mechanical performance, durability, leaching behavior, and LCA results, together with experimental parameters, curing conditions, and comparisons with OPC

ors (Year)	Binder / Material	Activator & Molarity	Curing	Test Methods	Key Findings (Strength / Durabi LCA)
llan et al., 11 [23]	Fly ash based geopolymer paste	NaOH + Na_2SiO_3 (various)	Ambient	Compressive strength, LCA	Comparable strength to OPC; 44–64% global warming potential (GWP) emi
uwan et al., 14 [24]	High-calcium fly ash paste	NaOH (8–18 M) + Na_2SiO_3	40°C	Setting time, compressive strength, electrical tests	Higher NaOH increased strength and time; enhanced geopolymerizati
., 2016 [25]	Slag-based cement	—	—	LCA	Slag substitution reduced global warm land-use impacts
et al., 2016 [26]	Fly ash-metakaolin paste	NaOH (9 M) + Na_2SiO_3	60–80°C (2–24 h)	Compressive strength	Optimal curing at 60° C-2 h; stren increased up to 25 MPa with 40%
l., 2017 [27]	Fly ash paste & mortar	NaOH + Na_2SiO_3	Ambient	Compressive strength, SEM, XRD	Strength governed by Si/Al ratio; m strength 23–26 MPa at 28 d of cu
et al., 2018 [28]	Geopolymer concrete (paste-based)	NaOH-based	Ambient	LCA	Up to 64% lower GWP than OPC co under optimized conditions
l., 2019 [29]	Fly ash geopolymer paste	Alkali solution (Na-based)	Ambient	Compressive strength, SEM	Optimized mix enhanced early streng microstructural densification
et al., 2019 [30]	Fly ash & metakaolin paste	Na_2SiO_3 + KOH	Ambient	Water absorption, porosity, strength	Better durability and corrosion resis than OPC paste
et al., 2020 [31]	GGBS/Metakaolin geopolymer mortar	NaOH + Na_2SiO_3 (MS 1.1–1.7)	Ambient	Flow, compressive strength	Optimum MS = 1.7; strength up to 7
i et al., 2021 [32]	Volcanic tuff pastes	NaOH / NaOH+Na_2SiO_3	23–150°C	Strength, setting time, SEM/XRD	NaOH activation resulted to superior s (41 MPa)
et al., 2020 [33]	Fly ash-GGBFS mortar	NaOH + Na_2SiO_3	Ambient	Strength, UPV	GGBFS enabled ambient curing; str increased up to 63 MPa
et al., 2022 [34]	Slag-silica fume mortar	Alkali activator + additives	10°C	Strength, SEM, FTIR	Early strength agents enhanced l temperature performance

ors (Year)	Binder / Material	Activator & Molarity	Curing	Test Methods	Key Findings (Strength / Durabi LCA)
hotri and a, 2022 [35]	Fly ash-GGBS mortar	NaOH + Na_2SiO_3	Ambient	Acid immersion, strength	Stable mass and strength up to 90 d s acid exposure
vent et al., 22 [36]	Metakaolin paste	NaOH + Na_2SiO_3	Immersio n (18 months)	Leaching, SEM, XRD	Limited Al leaching; stable minera
ander and ikala, 2022 [37]	Fly ash-GGBFS mortar	NaOH + Na_2SiO_3	Ambient	Durability, SEM, FTIR	Improved resistance to acid, sulfate chloride compared to OPC
arasan and a, 2023 [38]	GGBS paste	NaOH (1–8 M)	Ambient / oven	Strength, SEM/XRD	Ambient curing resulted to the hig strength (47 MPa)
l et al. 2023 [39]	copper mine tailings + Metakaolin	Alkali activator		Leaching, FTIR, XRD	Chemical stabilization mechanisms geopolymers
et al., 2024 [40]	Mine tailings + Steel slag	alkali hydrothermal activation	Ambient	Strength	Hydration products & C A S H form observed; microstructure studie
l., 2024 [41]	Geopolymer mortar	Alkali activator	Ambient	Flow, early-age strength	Achieved 44–55 MPa strength at 28 good flowability
et al., 2024 [42]	Metakaolin-slag paste + Carbon nanotube	NaOH + Na_2SiO_3	Water/se awater	Strength, SEM	Carbon nanotube increased strength 49.6 MPa
., 2024 [43]	Red mud-GGBFS paste/soil	Alkali activator	Ambient	UCS, TCLP	Enhanced strength and reduced heav leaching
l., 2023 [44]	One-part geopolymer paste	Solid Na-based activators	Acid immersio n	Strength loss, SEM, Mercury intrusion porosimetry (MIP)	Superior acid resistance with Na_2S activator
et al., 2025 [45]	Industrial waste + GGBFS + LS	NaOH (6–16 M)		Strength, SEM/XRD, FTIR, MIP	Microstructural characteristics (light aggregates)
ndez et al., 25 [46]	One-part geopolymer paste	Solid Na-silicate	Ambient	Leaching (Cesium, Strontium)	Better radionuclide retention than
et al., 2025 [47]	GGBFS geopolymer mortar	Alkali activator	Ambient	Strength, absorption, SEM	High mechanical strength and reduce absorption
et al., 2026 [48]	Mine tailings + slag blends	Na//K SiO + Na/K OH	Ambient / oven	Strength, TCLP	Achieved 30 MPa strength, Heavy m immobilized
is Work panipour et , 2026)	Iron ore tailings + GGBFS	NaOH (1–5 M)	Ambient / oven	Strength, TCLP , LCA	>90% heavy metal suppression, Mech linkage: N–A–S–H + C–A–S–H ge microstructure → strength, up to 35% GWP than OPC concrete

Accordingly, the primary objective of this study is to quantify the coupled mechanical and environmental behavior of alkali-activated IOT. This is achieved through a coordinated experimental program combining triaxial and consolidation testing with microstructural (SEM–EDS, XRD) and environmental (TCLP, LCA) analyses. Secondary analyses focus on the effects

of NaOH concentration and GGBFS replacement level, as well as the comparison of untreated, alkali-activated, and slag-modified systems.

Experimental program

A well-structured experimental matrix was developed to systematically examine the combined influence of three critical parameters: the concentration of the alkaline activator (NaOH), the proportion of GGBFS, and the curing period. The overall testing program is summarized in Table 2. This framework comprised three interrelated components:

- Mechanical evaluation, encompassing UU triaxial compression and one-dimensional consolidation tests;
- Environmental assessment, performed through TCLP;
- Microstructural characterization using SEM.

IOT served as the primary aluminosilicate precursor. Activation was achieved with NaOH solutions at three molarities, 1 M, 3 M, and 5 M to investigate the role of alkalinity in geopolymer reaction kinetics. To assess the influence of calcium on gel development, portions of IOT were substituted with GGBFS at replacement levels of 3, 6, and 9 wt%. These blended precursors were prepared and cast into test specimens for subsequent mechanical and environmental analyses.

Curing periods of 7, 14, and 28 days were applied to capture progressive changes in material strength and microstructural integrity associated with extended geopolymerization and secondary gel formation. Representative

samples from each curing stage were selected for consolidation tests, SEM observation, and TCLP leaching analyses.

This integrated experimental design provided a coherent and comprehensive understanding of how simultaneous variations in alkalinity, slag content, and curing duration govern the mechanical behavior, environmental stability, and microstructural evolution of alkali-activated tailing-based systems. The results ultimately reveal the interdependent mechanisms that control the strength development, durability enhancement, and stabilization performance of geopolymerized IOT.

For the UU triaxial compression tests, multiple specimens were prepared for each testing condition. Approximately 10% additional specimens were produced to ensure sample quality and suitability prior to testing, while about 20% of the specimens were tested in duplicate to verify the consistency of the measured shear strength parameters, resulting in 30% total repeatation of the tests. For the TCLP analyses, replicate tests were also conducted for Cu and Pb concentrations to assess the repeatability of the heavy metal measurements.

Table 2. Testing program for alkali-activated IOT under different NaOH concentrations, GGBFS contents, and curing times

Specimen Description	Curing Time (days)	Confining Pressure (kPa)	GGBFS Content (%)	NaOH Concentration (M)	Number of Specimens	Remarks
Reference (untreated IOT)	7	100, 200, 300	0	0	3	Baseline control sample
IOT + NaOH (No GGBFS)	7	100, 200, 300	0	1, 3, 5	9	Effect of alkali activation only
IOT + NaOH + GGBFS	7	100, 200, 300	3, 6, 9	1, 3, 5	27	Combined effect of alkali and GGBFS

IOT + NaOH (1 M, variable GGBFS content)	7, 14, 28	200	3, 6, 9	1	9	Effect of curing time at fixed NaOH concentration

Materials

The materials used in this study included IOT as the base material, GGBFS as the precursor, and NaOH as the alkaline activator. The tailings samples were collected from the Sourak iron mine tailings management facility located in Yazd Province, Iran.

To ensure consistent initial conditions, all samples were oven-dried at 60 ± 2°C for 72 h. The natural moisture content of the as-received tailings ranged between 29 and 38 percent. The optimum moisture content (11%) and maximum dry density (21.1 kN/m^3) of the tailings were determined using the standard Proctor compaction test (ASTM D698), and these values were subsequently used in specimen preparation.

The physical and mechanical properties of the tailings were obtained from a set of index tests, including Atterberg limits, standard Proctor compaction, and specific gravity of solids, as summarized in Table 3. Based on the unified soil classification system (USCS), the tailings are categorized as Low CL or low-plasticity clay.

As shown in Fig. 1, the particle size distribution curve clearly indicates the fine-grained character of the material. A considerable portion of particles passed through the No. 200 sieve with a size smaller than 75 µm, confirming

its clay-like texture, high compressibility, and pronounced deformation capacity under loading conditions.

Table 3. Physical and geotechnical properties of IOT

Property	Value	Standard/Method
Specific gravity (Gs)	3.25	ASTM D854[49]
Liquid limit (LL, %)	25	ASTM D4318[50]
Plastic limit (PL, %)	17	ASTM D4318[50]
Shrinkage Limit (SL, %)	13.2	ASTM D4943[51]
Plasticity index (PI, %)	8	ASTM D4318[50]
Soil classification	CL	ASTM D2487[52]
Optimum moisture content (w_{opt} , %)	11.0	ASTM D698[53]
Maximum dry density (γ_{dmax} , kN/m^3)	21.1	ASTM D698[53]

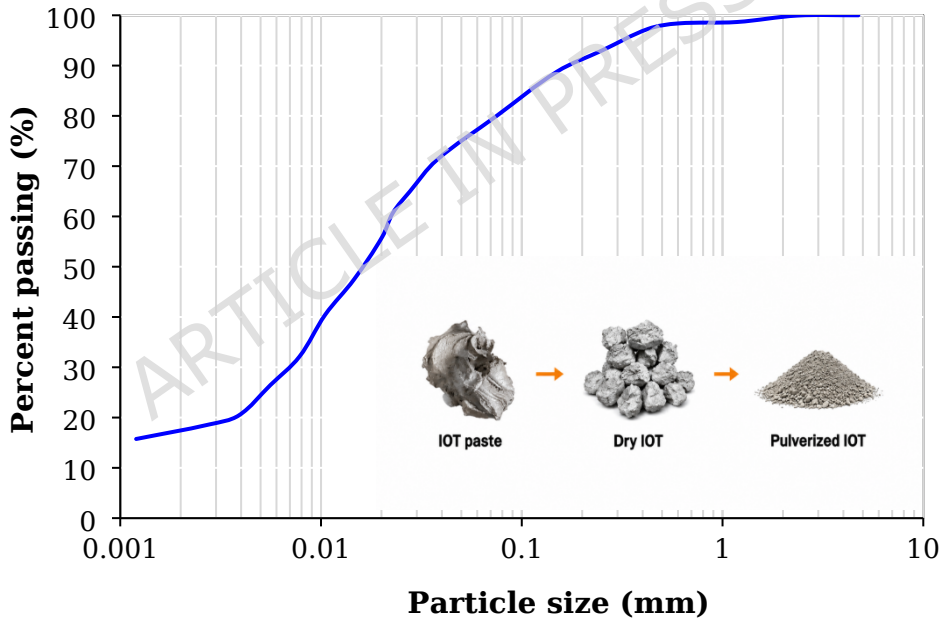

Figure 1. Particle size distribution curve of IOT

The XRD patterns of IOT and GGBFS, presented in Fig. 2, reveal distinct contrasts in their mineralogical composition and crystallinity. For tailings samples, the dominant crystalline phases identified were Goldmanite, Riebeckite, and Potassium Palladium Chloride, indicating the presence of

silicate and ferritic frameworks with reactivity potential by alkaline activation.

The identification of Riebeckite and Goldmanite as Fe-bearing silicates and aluminosilicates suggests the existence of partially soluble components capable of contributing to the formation of alkali-aluminosilicate gels (Na–Al–Si–H). Moreover, the coexistence of transition elements such as Fe and Al within these structures enhance geopolymerization kinetics through localized catalytic effects, thereby increasing the reactivity of tailings under alkaline conditions.

In contrast, the XRD pattern of GGBFS exhibits sharp and intense diffraction peaks corresponding to silicon oxide, calcium silicate, calcium aluminum silicate, and pyroxene phases, confirming its substantially higher alkaline reactivity and a strong tendency to form secondary binding products. The Ca–Si–Al phases readily dissolve and reprecipitate in the presence of NaOH, leading to the development of stable Ca–Al–Si–H gel networks that improve microstructural densification, interparticle bonding, and mechanical strength in the geopolymeric matrix.

A comparative evaluation of the phase assemblages of the two precursors shows that although IOT contain moderately reactive silicate phases, GGBFS demonstrates significantly greater chemical reactivity, owing to its abundance of calcium-rich and aluminosilicate phases, as well as a pronounced amorphous fraction. These features render slag an exceptionally effective participant in geopolymerization reactions, accelerating the

formation of binding gel phases and enhancing the mechanical and microstructural properties of blended systems.

Nevertheless, the patterns illustrated in Fig. 2 reveal a considerable mineralogical resemblance between IOT and GGBFS, suggesting that despite their comparatively lower reactivity, the tailings retain sufficient potential to function as reliable precursors in alkali-activated and geopolymeric formulations.

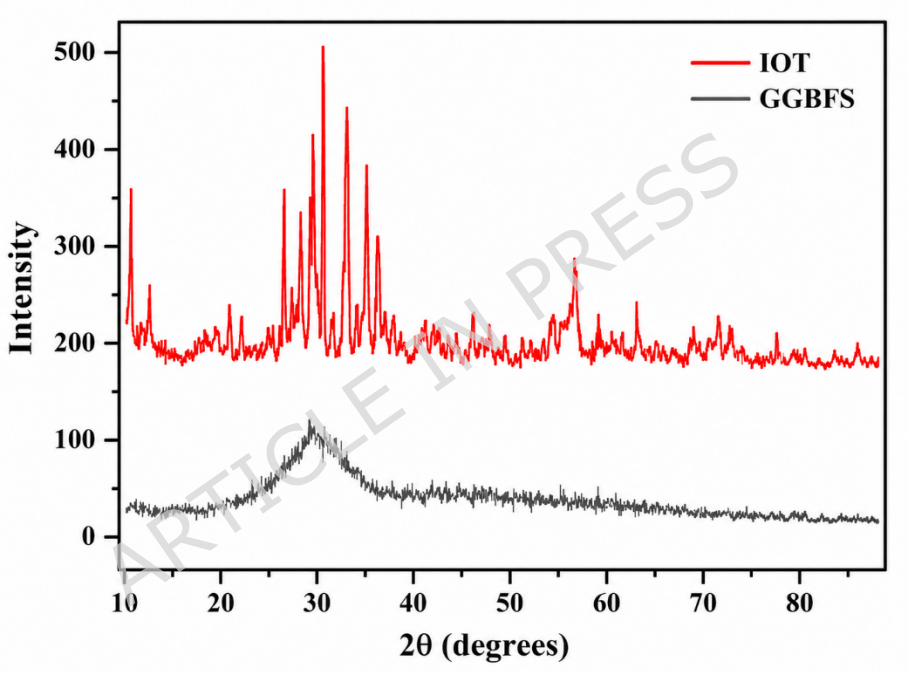

Figure 2. XRD patterns: (a) IOT, (b) GGBFS

Complementary evidences from XRF analysis, summarized in Table 4, further validates the mineralogical interpretations derived from XRD results. The chemical composition of the IOT primarily consists of silica (SiO_2), alumina (Al_2O_3), and iron oxide (Fe_2O_3), while the slag displays higher proportions of calcium- and silicate-bearing compounds, confirming its Ca-rich and reactive nature. This compositional trend correlates closely with the crystalline

phases observed in XRD, substantiating the coexistence of Fe–Si dominated phases in the tailings and Ca–Al–Si phases in the slag. The elevated contents of CaO and MgO in slag enhance its alkaline reactivity, facilitating the generation of calcium–aluminosilicate–hydrate (Ca–Al–Si–H) gels under NaOH activation. In contrast, the higher proportions of SiO_2, Fe_2O_3, and Al_2O_3 in the tailings favors the formation of alkali–aluminosilicate (Na–Al–Si–H) gel networks. Such compositional contrasts critically govern the dissolution behavior, reaction kinetics, and microstructural evolution of secondary phases, thereby determining the hardening and consolidation mechanisms of the activated system.

The alkaline activator solutions were prepared using NaOH pellets with 98% purity and a molecular weight of 40 g/mol. Solutions of 1, 3, and 5 M concentrations were obtained by precisely weighing the required NaOH mass (accuracy ± 0.001 g) and dissolving it in distilled water. Due to the exothermic nature of NaOH dissolution, each solution was left to stabilize at ambient conditions for 24 hours prior to use, ensuring complete equilibration of ionic species. The highly alkaline environment generated by NaOH promotes partial dissolution of silicate and aluminosilicate phases in both the tailings and slag, effectively initiating and accelerating geopolymerization reactions. The resulting three-dimensional aluminosilicate framework forms a compact and cohesive matrix, providing the solidified composites with their fundamental mechanical strength, durability, and chemical stability. In addition, NaOH was selected as the alkaline activator due to its demonstrated

effectiveness in generating the highly alkaline environment required for aluminosilicate dissolution. Its widespread availability and established use in previous studies make it a suitable and consistent choice for comparative analysis. Compared to more complex activator systems, the use of NaOH provides a simpler and more field-applicable stabilization approach.

Table 4. XRF Results for comparison of IOT and GGBFS components

Component	IOT (wt%)	GGBFS (wt%)	Component	IOT (wt%)	GGBFS (wt%)
SiO_2	40.09	35.9	BaO	1.02	2.1
CaO	17.93	38.2	MnO_2	0.29	1.5
MgO	9.83	8.9	P_2O_5	0.26	0.32
Al_2O_3	6.05	8.62	Ni	0.02	-
Fe_2O_3	22.38	0.76	Cu	0.03	-
SO_3	1.64	0.7	Zn	0.01	-
K_2O	0.11	0.7	Pb	0.04	-
TiO_2	0.28	1.9	Sr	0.02	0.4
LOI	2.32	0.9			

Methods

Specimen casting and curing conditions

Cylindrical specimens with an internal diameter of 38 mm and a height of 120 mm were prepared to evaluate their mechanical performance under controlled laboratory conditions. After compaction, the specimens were carefully demolded and trimmed to a final height of 80 mm, ensuring uniform geometry and consistent dimensions.

The specimens were prepared at 100% relative compaction using the optimum moisture content (w_{opt}) determined from the standard Proctor test (ASTM D698). The corresponding maximum dry unit weight ($\gamma_{d\,max}$) was used

to calculate the required dry mass for each specimen. The mixtures consisted of finely pulverized IOT, partially replaced by GGBFS at 3%, 6%, and 9%. Alkali activation was performed using NaOH solutions with molar concentrations of 0, 1, 3, and 5 M, serving as the sole liquid phase. The total liquid content was fixed at the optimum moisture content (11%), corresponding to a liquid-to-solid ratio of 0.11. Material quantities were determined based on specimen volume and maximum dry unit weight, with all proportions defined on a dry mass basis. It should be noted that this ratio was kept constant during the preparation of samples with different NaOH solution molarities and GGBFS contents. No independent binder phase was defined, as the system was predominantly tailings-based with relatively low GGBFS content. Accordingly, GGBFS was treated as a supplementary reactive component, and the liquid-to-binder ratio was assumed equivalent to the liquid-to-solid ratio considering the unit weights of NaOH and GGBFS. In this regard, the total solids content for all mixtures was approximately 90%.

Mixing was performed using a mechanical agitator for approximately 2 minutes to ensure uniform distribution of the activator and homogeneous mixing. The mixtures were placed into cylindrical molds in three successive layers, each statically compacted and lightly scarified to promote proper interlayer bonding.

After demolding, specimens were sealed in airtight polyethylene bags to limit moisture exchange and prevent drying shrinkage, and then cured at 30 ± 2 °C for 7, 14, and 28 days. The curing temperature of 30 ± 2 °C was selected

to simulate ambient curing conditions commonly encountered in practical geotechnical applications. This temperature range allows geopolymerization to proceed under realistic conditions without artificial thermal acceleration, while also being representative of typical environmental conditions in many regions, including the study area [40, 54].

Finally, specimens were selected based on dimensional tolerance (±1.5%), dry-mass stability (±1%), and consistency in moisture condition to ensure test uniformity and reproducibility.

Unconsolidated undrained (UU) triaxial test

Unconsolidated–undrained (UU) triaxial tests were performed in accordance with ASTM D2850-15 to evaluate the short-term shear characteristics and undrained strength response of the geopolymer-stabilized specimens. The UU testing procedure was selected as a widely accepted approach for evaluating the undrained shear strength of geomaterials under total stress conditions. This method was selected to simulate field conditions, where materials are typically compacted at or near their optimum moisture content rather than under fully saturated state. All samples were compacted at their respective optimum moisture content and were not subjected to any pre-saturation process prior to loading, ensuring that their moisture state remained within a partially saturated range during testing. This approach is consistent with common practice for compacted fills and tailings [9, 55, 56]. All specimens were prepared using a consistent compaction procedure and shear strength parameters were calculated based on total stress concept.

During specimen preparation, each sample was molded at the optimum moisture content using either distilled water or NaOH activating solution, depending on the formulation. After curing, the specimens were meticulously mounted on the triaxial apparatus pedestal, and a standard-thickness latex membrane was carefully placed to isolate the sample from the confining fluid. The lower end of the membrane was secured using rubber O-rings, followed by the precise alignment of the top cap and completion of the upper sealing to ensure an airtight enclosure.

After the triaxial cell was assembled, confining pressure was applied while all drainage valves were kept fully closed to maintain undrained conditions. The tests were conducted under three different confining pressures, 100, 200, and 300 kPa to represent varying stress environments. Deviatoric loading was applied under strain-controlled conditions at a constant axial deformation rate of 1 mm/min, allowing for uniform stress development across the specimens.

Throughout the testing process, axial force and vertical strain were continuously monitored and recorded using a digital data-acquisition system. Axial load measurements were obtained through an electronic load cell, while a calibrated transducer verified cell pressure stability. It should be noted that pore water pressure was not measured during testing; therefore, the shear strength parameters are interpreted in terms of total stress conditions. The specimens were tested at their as-compacted moisture condition to better

simulate practical engineering conditions. Indeed, the partially saturated condition of the specimens is consistent with field conditions in compacted geomaterials [57, 58].

Leaching tests

The leaching behavior of heavy metals immobilized within the geopolymer matrix was assessed using the TCLP in accordance with U.S. EPA Method 1311, to evaluate the chemical stability and environmental safety of the stabilized samples. Cured specimens were crushed to achieve a uniform particle size and passed through a 9.5mm sieve, ensuring full compliance with the standard requirements [59].

For each test, 20 g of the prepared sample was mixed with Extraction Fluid No. 2, which consisted of 0.1 M acetic acid buffered at pH 2.88 ± 0.05, with a solid-to-liquid ratio of 1:20 (g/mL). This acidic fluid was explicitly chosen to replicate the leachate conditions of municipal landfills, providing a realistic chemical challenge for the inherently alkaline geopolymer materials.

The suspensions were placed in borosilicate glass bottles resistant to chemical attack and agitated for 18 hours at ambient temperature using a mechanical shaker operating at 30 rpm. After the agitation period, the contents were filtered through 0.45µm membrane filters, and the resulting filtrates were immediately transferred to pre-acidified containers (pH < 2) to prevent post-filtration precipitation or compositional alteration.

The dissolved heavy metal concentrations were measured using atomic absorption spectroscopy. The results were compared with those of the

untreated tailings, revealing a substantial decrease in metal mobility due to geopolymerization and the development of stable Na–Al–Si–H and Ca–Al–Si–H binding phases within the solid matrix.

One-dimensional consolidation tests

One-dimensional consolidation tests were conducted following the procedures described in ASTM D2435 to examine the influence of alkaline activator concentration and slag incorporation on the compressibility characteristics of geopolymer-stabilized IOT. Cylindrical specimens measuring 50 mm in diameter and 17 mm in height were carefully prepared using materials adjusted to an initial moisture content of 13.2%, as determined from the shrinkage-limit test, to provide a controlled initial moisture condition while avoiding excessive volume change during specimen preparation. Each sample was trimmed to a final height of 17 mm within consolidation rings of 50 mm internal diameter and 20 mm height, corresponding to approximately 70% of maximum unit weight based on the standard Proctor test results.

A control specimen without NaOH was prepared to serve as a baseline for isolating the effects of alkaline activation. For all activated samples, 7.15 g of deionized water containing NaOH at different molarities was mixed with the dry material, resulting in a uniform initial void ratio of 0.945 for all specimens at early-age.

After placement, each specimen was immediately submerged in water and maintained under submerged conditions for 24 hours, allowing for moisture

equilibration under the intended testing condition. Vertical stresses of 100, 200, 400, and 800 kPa were imposed sequentially, followed by unloading stages in which the applied stresses were decreased to 400 kPa and subsequently to 200 kPa.

During the entire consolidation process, settlement was recorded as a function of logarithmic time, enabling the derivation of compression and swelling indices (Cc and Cs) from the typical void ratio versus effective stress (e–log σ′) plots. This systematic approach aimed to elucidate how alkali concentration and slag addition govern compressibility, settlement response, and the evolution of an overconsolidated geopolymer structure within the stabilized tailings matrix. The adopted testing condition was intended to simulate the post-deposition behavior of tailings after material extraction, where they are commonly stored in a soft or slurry state and undergo consolidation under fully saturated conditions for an extended period.

pH and electrical conductivity measurements

The chemical environment of the stabilized matrix was evaluated through systematic measurements of pH and electrical conductivity (EC), in accordance with ASTM D 4972-01, which provided insight into the evolving pore solution chemistry throughout the geopolymerization process. Air-dried samples were finely pulverized until passing completely through a No. 10 sieve (2.0 mm opening) to obtain homogeneous test materials [60, 61].

A suspension was prepared by mixing 10 g of the processed material with 10 mL of deionized water, maintaining a controlled solid-to-liquid ratio of 1:1

(g/mL). The mixture was manually stirred for 5 minutes to achieve complete dispersion and then allowed to equilibrate for 1 hour at ambient temperature, ensuring stabilization of the ion-exchange reactions between the solid and liquid phases [61].

After equilibration, the supernatant solution was carefully decanted, and measurements of pH and EC were recorded using properly calibrated digital meters to ensure reproducibility and precision. These values served as key indicators of the system's alkalinity and ionic mobility, directly reflecting the progression of dissolution–polycondensation phenomena that govern the development of Na–Al–Si–H and Ca–Al–Si–H gel networks in the geopolymer matrix.

Microstructural analysis (SEM–EDS)

Microstructural analyses were performed using SEM to investigate the morphological evolution, microstructural features, and possible reaction products within the geopolymer-stabilized matrix. Representative fragments were meticulously extracted from specimens encompassing the complete range of experimental variables, namely NaOH activator concentrations of 0, 1, 3, and 5 M, and GGBFS substitution levels of 3, 6, and 9% (by dry mass). After mechanical testing, the samples were cut into cubes with edge lengths of approximately 50 mm, and the surfaces were carefully cleaned of dust and debris before coating. This systematic sampling approach ensured that the SEM observations captured the progressive microstructural transformations induced by varying alkaline activation and calcium availability, thereby

providing a comprehensive basis for correlating morphological features with the underlying geopolymerization mechanisms.

Prior to imaging, the fractured surfaces were sputter-coated with a uniform layer of gold using a coating device. The SEM–EDS system used was a ZEISS microscope located at the Central Microscopy Laboratory, Kharazmi University, Tehran. The SEM–EDS analyses were conducted under high-vacuum conditions using an accelerating voltage of 16 kV and a field emission electron source to achieve high resolution. The working distance, detector type, and imaging parameters were optimized to clearly visualize micro-textures and bonding regions within the geopolymeric network.

It should be noted that SEM provides two-dimensional representations of the material microstructure. Therefore, the observations primarily reflect surface morphology and are used for qualitative interpretation and comparative assessment of microstructural features. In this context, the porosity values obtained are also interpreted as two-dimensional estimations and are primarily used for comparative purposes among different samples. Accordingly, these values do not necessarily represent true volumetric porosity and may not fully capture the three-dimensional pore structure.

To complement the qualitative observations, a semi-quantitative assessment of pore distribution was performed using ImageJ software on grayscale SEM images. The image processing procedure included conversion to 8-bit format, contrast enhancement, and threshold-based segmentation to distinguish pore regions from solid phases. The threshold values were selected based on visual

calibration to achieve an optimal distinction between darker pore areas and brighter solid regions.

This investigation focused on identifying the formation and distribution of geopolymer reaction products, particularly the development of Na–Al–Si–H and Ca–Al–Si–H gel phases, and on evaluating interparticle adhesion and matrix densification in relation to activator molarity and slag content. SEM observations provide a reliable basis for describing and comparing microstructural features associated with geopolymerization, although their interpretation remains within the scope of morphological characterization.

Results and discussion

Compaction characteristics

To establish the baseline parameters for specimen preparation, the standard Proctor compaction test (ASTM D698) was first performed on untreated IOT (i.e., without any additive). The results indicated that γ_{dmax} was 21.1kN/m^3, while w_{opt} reached 11.0%. Consoli et al. suggested adopting the values obtained for untreated soil as a quality-control references for the preparation of all subsequent blends, including different GGBFS values, to eliminate density as a confounding variable and ensure uniform compaction energy across all mixtures [54]. However, in present study, compaction tests were conducted on GGBFS-amended mixtures to assess the impact of slag incorporation on their physical compaction properties. As summarized in Table 5, increasing the GGBFS content resulted in a gradual decline in γ_{dmax}, accompanied by a corresponding increase in w_{opt} [62, 63]. This consistent

trend arises from the gradual replacement of relatively coarse and dense tailings particles with finer, lighter, and predominantly amorphous slag grains. Owing to their finer particle size, distinct particle size distribution, and glassy amorphous structure, slag particles provide a larger effective contact area within the mixture. Although the paste tailings themselves exhibit a considerable surface area, the increase in water demand and the consequent rise in the optimum moisture content cannot be attributed solely to specific surface area; rather, it primarily results from the combined effect of slag fineness and its packing characteristics within the mixture, which require greater water availability for the initiation and progression of alkaline activation reactions [64, 65]. Comparable behavior has been reported in previous studies on pozzolanic stabilization of fine-grained soils and mining tailings [66]. From a geotechnical standpoint, the reduction in maximum dry density indicates lower physical compressibility. However, the simultaneous increase in optimum moisture content provides a reactive environment conducive to the formation of gel-like binding phases, such as Ca–Si–H and Na–Al–Si–H, during geopolymerization [67]. Consequently, although higher slag content slightly diminishes mechanical compaction efficiency, this drawback is effectively counterbalanced by the enhanced chemical reactivity, which promotes the formation of durable cementitious and pozzolanic networks within the geopolymer matrix.

Table 5. Standard compaction test and specific gravity test results for tailings and GGBFS containing mixtures

Sample	GGBFS (%)	G_s (g/cm³)	γ_{dmax} (kN/m³)	w_{opt} (%)
IOT	0	3.25	21.1	11.0
IOT + GGBFS	3	3.23	20.9	11.4
IOT + GGBFS	6	3.20	20.6	11.8
IOT + GGBFS	9	3.16	20.3	12.1

Shear strength characteristics of the stabilized tailing

As illustrated in Figs. 3 and 4, both the activator concentration (NaOH molarity) and the GGBFS content exert a dominant influence on the mechanical enhancement and final strength of the geopolymer-stabilized matrix. Figure 3 presents the variation of peak deviatoric stress as a function of NaOH concentration (0, 1, 3, and 5 M) under confining pressures of 100, 200, and 300 kPa. The trend exhibits a distinctly nonlinear and asymptotic pattern, reflecting the interplay between the kinetics of geopolymerization reactions and the level of mechanical confinement.

A pronounced strength escalation occurs within the low-alkalinity range of 0–1 M, where the rate of strength gain is at its maximum. For instance, at a confining pressure of 100 kPa, the deviator stress increases from approximately 335 to 839 kPa, representing a nearly 250% increase. A sudden increasing trend is observed under 300 kPa confinement, where the strength nearly doubles, rising from 580 to 1086 kPa. This sharp initial gain marks the onset of effective alkaline activation, during which the elevated pH accelerates the hydrolysis of covalent bonds within aluminosilicate precursors, producing a supersaturated solution rich in silicate and aluminate species. Such a reactive environment promotes nucleation and

growth of Na–Al–Si–H gels [68, 69], while the availability of calcium from the tailings further facilitates the development of hybrid phases that reinforce interparticle bonding [70, 71], which is in agreement with the mechanism reported by Huang et al. (2024).

The results further indicate that the effect of NaOH is not limited to slag-containing systems. Even in the absence of slag, the addition of NaOH leads to noticeable improvements in mechanical performance, suggesting intrinsic activation of the mineral phases present in the tailings and highlighting the independent role of NaOH in modifying the internal structure of the system. At NaOH concentrations exceeding 1 M, the system enters a regime of diminishing efficiency. Although the absolute strength continues to increase, reaching approximately 1150 kPa at 100 kPa confinement and 1480 kPa at 300 kPa confinement for 5 M NaOH, the rate of strength gain becomes markedly reduced. This decline in efficiency can be attributed to the saturation of dissolution reactions, accumulation of unreacted ionic species, and diffusion limitations within the increasingly dense reaction medium [70].

Finally, beyond chemical effects, the vertical separation of the strength curves in Fig. 3 highlights the independent contribution of confining pressure. Across all activator concentrations, increasing the confining pressure from 100 to 300 kPa results in an additional strength gain of approximately 100–200 kPa, which can be attributed to pore compaction and enhanced frictional interlocking between particles.

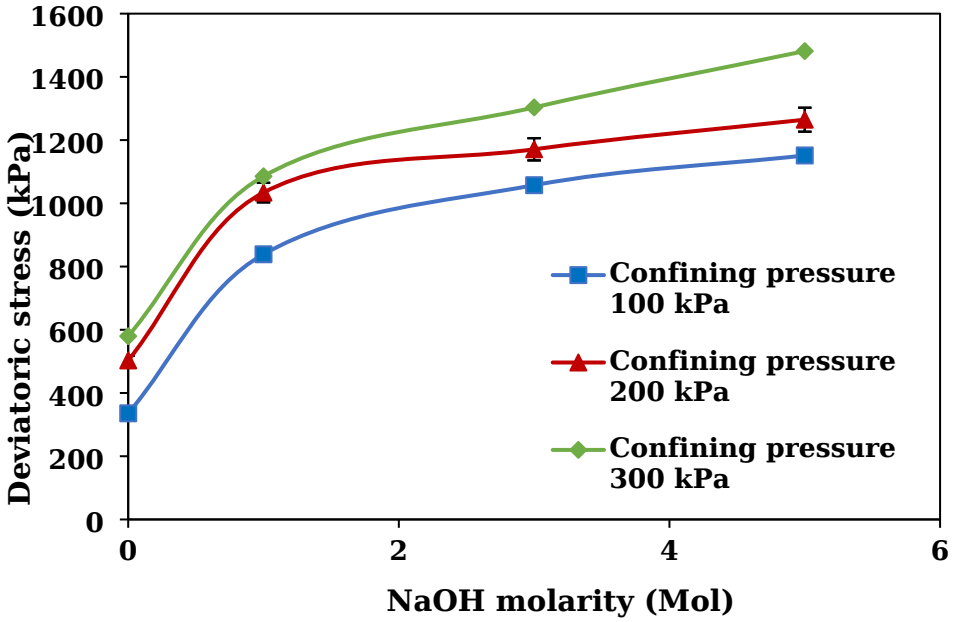

Figure 3. Effect of activator molarity on the peak strength of treated tailing

Impact of GGBFS content on strength behavior

The mechanical evolution of stabilized IOT as a function of GGBFS incorporation is presented in Fig. 4. These plots compare the compressive strength under varying NaOH molarities (1, 3, and 5 M) across three replacement levels of 3, 6, and 9% GGBFS for three confining pressures.

The comparative analysis reveals that strength enhancement is directly governed by the interplay between slag dosage and alkaline concentration. Under low alkalinity (1 M), the differences among specimens remain small, for example 1370, 1640, and 1810 kPa for 3, 6, and 9% GGBFS, respectively at 200 kPa confinement. This narrow band (≈10–20%) reflects insufficient alkalinity to dissolve the amorphous phases of GGBFS, creating a kinetic bottleneck that restricts reaction progression and limits early-stage geopolymerization (Consoli et al. 2020).

At higher molarities (3 and 5 M), however, strength envelopes diverge sharply, exhibiting a distinctive “fan-like” behavior. At 200 kPa confinement, the specimen with 9% GGBFS demonstrates a dramatic escalation from ≈4110 kPa at 3 M to ≈5824 kPa at 5 M, while the 3% series peaks near ≈3330 kPa, even under the same conditions. This ≈75% disparity underscores a pronounced synergetic interaction between activator molarity and slag dosage, confirming that higher $CaO–SiO_2–Al_2O_3$ content within GGBFS substantially strengthens the matrix when alkalinity is adequate. Quantitatively, the average strength-gain rate within the 0–3 M range for the 9% series (≈980 kPa/M) outpaces that of the 3% series (≈630 kPa/M) by roughly 1.5 times, further evidencing accelerated dissolution and efflorescence kinetics.

This marked increase arises from the high reactivity of GGBFS, an amorphous, calcium-rich precursor that dissolves rapidly under strong alkaline conditions, promoting precipitation of (Ca–Al–Si–H) and complementary (Na–Al–Si–H) gel phases [72]. Moreover, the MgO present in GGBFS has been shown to reinforce the geopolymer matrix and retard micro-cracking, contributing to greater load transfer efficiency [73].

The fan-like divergence of the curves effectively delineates a threshold alkalinity requirement for unlocking the full potential of high-slag formulations. The benefit of slag addition becomes dominant only when the activator concentration exceeds the kinetic threshold, enabling sustained polymerization. Conversely, the flattening of the curves beyond 3 M for low-

slag mixes (3%) signifies entry into a “precursor-limited” regime, where reactive aluminosilicate species become depleted, and further increases in NaOH concentration yield negligible mechanical returns [70].

It is worth emphasizing that even the unreacted slag (for GGBFS content more than 9%) contribute indirectly to strength enhancement, acting as micro-reinforcing inclusions that promote gel–particle interlocking and facilitate more efficient stress transfer throughout the geopolymeric framework [20]. Taken together, these observations indicate that optimum mechanical performance is achieved within a balanced activation regime, characterized by moderate alkalinity (≈approximately 3 M) and elevated slag content (approximately 9%). Under such conditions, the matrix evolves into a denser and more over-consolidated binding network, capable of attaining compressive strengths exceeding 5.8 MPa, thereby reflecting the synergistic interplay between physical densification and chemical bonding processes that govern geopolymer stabilization.

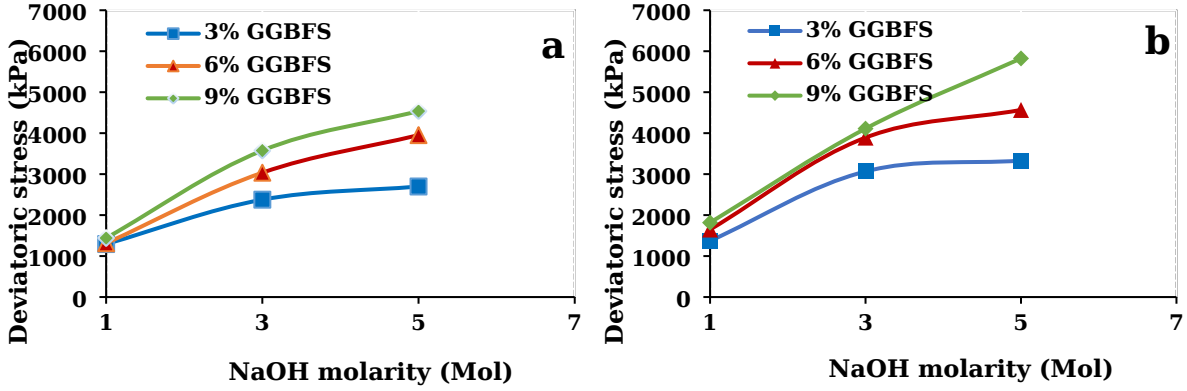

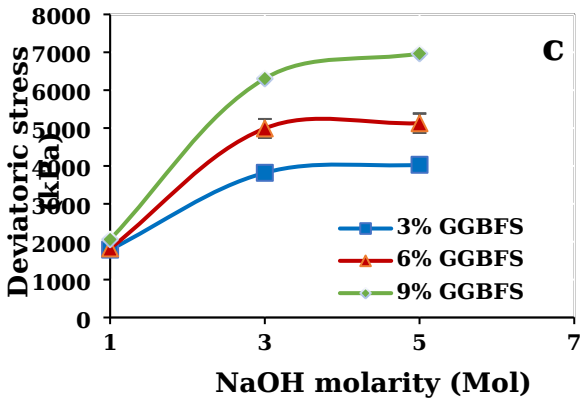

Figure 4. Effect of GGBFS content on strength at different confining pressures, (a) 100 kPa, (b) 200 kPa, (c) 300kPa

Temporal evolution of strength and curing effects

Experimental results clearly demonstrate that the curing period plays a crucial role in determining the progressive mechanical development of the geopolymer matrix. As depicted in Fig. 5, all mixtures exhibit a consistent increase in compressive strength between 7 and 28 days; however, the magnitude of this improvement is highly dependent on the incorporated slag content. Notably, the specimen containing 9% GGBFS demonstrated a remarkable threefold increase in compressive strength, from approximately 1816 kPa at 7 days to over 6260 kPa at 28 days, representing the most pronounced strength evolution among all tested formulations. This trend highlights the crucial role of calcium-rich slag in promoting long-term geopolymerization and densification processes during extended curing periods.

Analysis of strength-time gradients reveals distinct kinetic mechanisms. Mixtures with low GGBFS content (3% GGBFS) rapidly attain >80% of their final strength within the first 14 days, indicating fast consumption of

available reactants and early structural saturation. In contrast, high-GGBFS blends (6% and 9% GGBFS) exhibit a prolonged upward trajectory up to 28 days, suggesting extended dissolution–precipitation cycles and sustained polymeric reorganization. This behavior typifies high-calcium alkali-activated systems, in which latent hydration and geopolymerization phases coexist, producing progressive densification and enhanced micro-structural integrity [74, 75].

This progressive hardening of the geopolymer matrix is driven by sustained geopolymerization kinetics within a calcium-rich medium. Early curing is dominated by the rapid formation of the sodium-aluminosilicate-hydrate (Na–Al–Si–H) network, establishing initial cohesion among particle clusters. As curing continues, the dissolution of GGBFS releases Ca^{2+} ions, promoting the formation of secondary (Ca–Al–Si–H) and hybrid (Na–Ca–Al–Si–H) phases that densify the matrix, fill residual porosity, and refine particle interfaces. Extended curing not only increases overall strength but also transforms the system from an Na–Al–Si–H–dominated network into a calcium-integrated composite (Ca–Al–Si–H and Na–Ca–Al–Si–H) with enhanced stiffness, structural integrity, and durability. The progressive consolidation and reduction in volumetric strain confirm that inter-particle bonds are reinforced and gel frameworks are fortified, resulting in a load-responsive composite suitable for geotechnical stabilization applications [60, 76, 77].

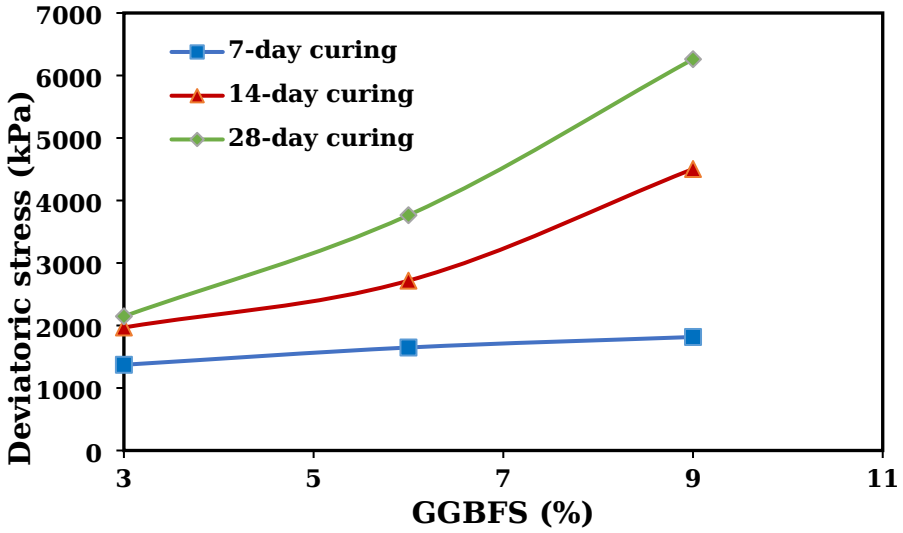

Figure 5. Influence of curing time on strength at fixed confined pressure of 200 kPa and 1M NaOH

These results strongly corroborate the earlier findings of Nath and Sarker (2015), who demonstrated that prolonged curing in GGBFS activated systems promotes gradual micro-structural densification and maturation of the geopolymer network by steadily reducing interconnected porosity.

Shear strength parameters

Experimental results from unconsolidated undrained triaxial tests clearly demonstrate that both the alkali activator concentration (NaOH) and the dosage of GGBFS play decisive roles in determining the cohesive strength of the geopolymer-stabilized mixtures. As illustrated in Fig. 6, increasing the NaOH molarity from 0 to 5 M in the absence of GGBFS elevated the cohesion from approximately 80 kPa to about 320 kPa. This fourfold enhancement is attributed to the extensive development of Na–Al–Si–H gel networks, which promote interparticle bonding and ensure the structural integrity of the geopolymer matrix [78, 79].

When GGBFS was incorporated into the system, the rate of cohesion growth intensified significantly. Figure 6 clearly highlights this synergistic behavior, where the simultaneous increase in NaOH molarity and slag content results in a nonlinear amplification of cohesive strength. Specifically, under a 5 M alkaline environment, increasing the GGBFS content from 0% to 9% resulted in a significant increase in cohesion from approximately 320 kPa to over 750 kPa. This sharp rise underscores the crucial role of calcium ions (Ca^{2+}) in promoting the formation of secondary Ca–Al–Si–H and Na–Ca–Al–Si–H phases, which fill the internal voids and densify the matrix skeleton, thereby optimizing structural continuity [80].

Furthermore, the steeper slope of the cohesion curves at higher molarities, compared to non-GGBFS mixtures, confirms a strong synergistic interaction between NaOH activation and slag enrichment. The coexistence of a highly alkaline environment and calcium-rich precursors accelerates the geopolymerization kinetics, thereby maximizing the matrix cohesion.

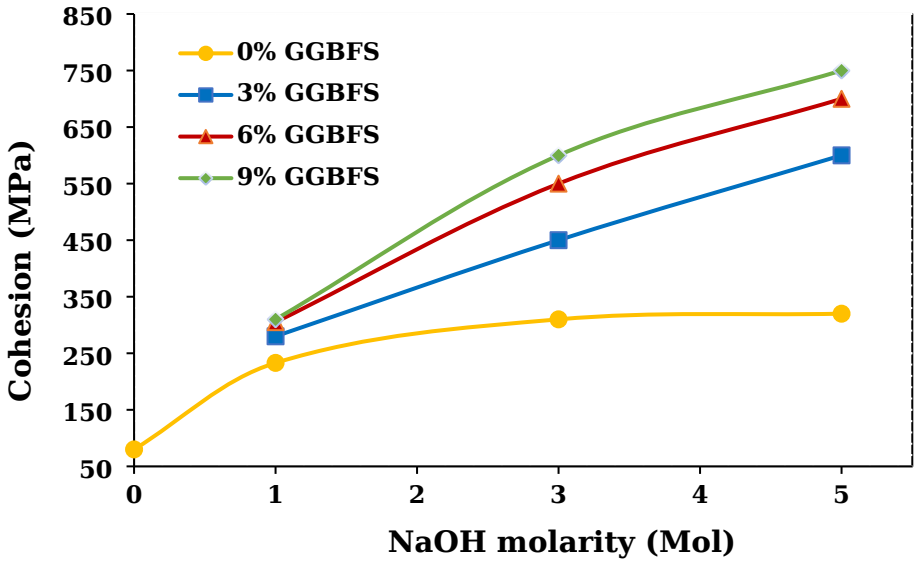

Figure 6. Effect of alkaline molarity on the induced cohesion of IOT

The variation of the internal friction angle (φ) reveals that, although its overall trend is generally consistent with that of cohesion, the magnitude and sensitivity of the response differ significantly with respect to the experimental variables. As illustrated in Fig. 7 for mixtures without GGBFS, increasing the NaOH concentration from 0 to 5 M had only a limited influence on the frictional response, with φ increasing slightly from approximately 21.18° to 25.64°. This relatively modest increase suggests that the alkaline environment primarily enhances chemical bonding and apparent cohesion but exerts limited influence on the intrinsic surface texture or interparticle frictional behavior of the tailings.

Conversely, the inclusion of GGBFS markedly altered the shear response of the mixtures. Under strongly alkaline conditions (5 M NaOH), increasing the slag content from 0% to 9% resulted in a remarkable increase in the internal

friction angle, from approximately 25.6° to nearly 50°. We attribute this substantial enhancement to the combined physicochemical contribution of GGBFS: chemically, it participates in geopolymeric and cementitious reactions and contributes to the formation of rigid gel phases (C–A–S–H and N–C–A–S–H), thereby strengthening interparticle cohesion and matrix integrity. As cementation progresses, individual particles tend to form bonded aggregates or block-like structures. Consequently, during shearing, the failure mechanism gradually shifts from simple sliding between fine particles to frictional sliding and rearrangement between larger cemented blocks. This transition substantially increases resistance against shear deformation and contributes to the development of unusually high friction angles. Physically, its angular morphology and rough surface texture increase interlocking efficiency among particles and restrict relative displacement. This combined chemical–mechanical reinforcement effectively restricts relative sliding, resulting in a pronounced improvement in the overall shear resistance and strength development [79].

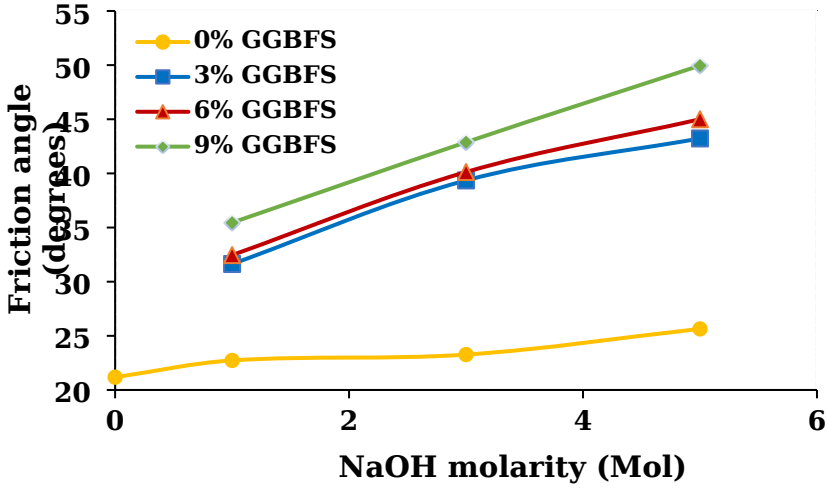

Figure 7. Effect of alkaline molarity on the induced friction angle of IOT

Evolution of pH and EC

Simultaneous monitoring of pH and EC provided valuable insights into the reaction kinetics and ionic evolution within the stabilized geopolymer system. As depicted in Fig. 8, both parameters exhibited a correlated yet nonlinear response to the replacement ratio of GGBFS. At moderate activator concentrations (3 M NaOH), increasing the slag content to 6% resulted in a pronounced rise in alkalinity and conductivity, accompanied by a corresponding increase in pH from 9.5 to 12.6. In contrast, EC increased from 14.4 to 22.3 mS/cm. This behavior can be attributed to the rapid dissolution of amorphous slag phases and the subsequent release of reactive ionic species such as Ca^{2+}, Mg^{2+}, $Si(OH)_4$, and $Al(OH)_4^-$, which collectively enhance the ionic strength and accelerate the nucleation of Ca–Si–H and Na–Al–Si–H gels [81].

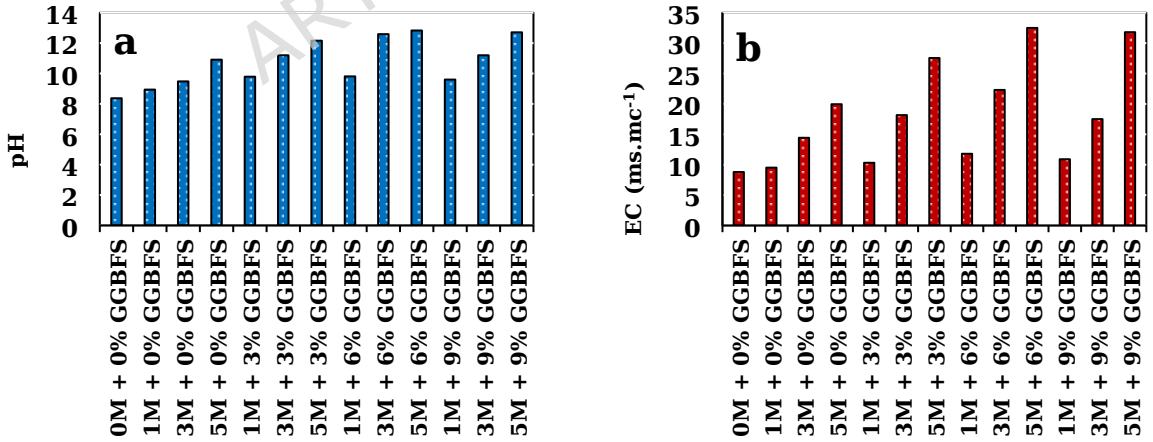

Figure 8. Variations of (a) pH and (b) EC with GGBFS content and NaOH molarity

However, at a higher slag content of 9%, an opposite trend emerged, with pH and EC values decreasing to approximately 11.2 and 17.5 mS/cm, respectively. We interpret this decline not as a loss of reactivity, but as an indication of a shift in reaction regime, from dissolution-dominated to condensation-dominated behavior. In the presence of abundant reactive precursors, the consumption rate of hydroxyl (OH^-) and sodium (Na^+) ions during the formation of the geopolymeric framework surpasses their rate of release. Consequently, free ions responsible for high alkalinity and conductivity become immobilized within the hardened matrix or incorporated into stable Ca–Al–Si–H phases [82].

The concurrent reduction in pH and EC alongside the notable increase in compressive strength further supports this interpretation, suggesting the structural maturation of the system. As observed by Blotevogel et al., this behavior reflects the effective immobilization of mobile ions within the polymeric network. This mechanism results in a denser structure, ensuring the long-term chemical and mechanical stability of the stabilized tailings.

Although pH and EC provide valuable insights into the ionic environment of the system, it should be noted that redox conditions (Eh) may also influence the chemical stability and mobility of iron and trace metals in tailings. However, considering the highly alkaline conditions of the present study, the system is expected to be dominated by pH-controlled mechanisms, and redox effects are assumed to play a secondary role.

A comprehensive assessment of the stabilized tailings reveals that simultaneous increments in NaOH concentration and GGBFS content decisively enhance mechanical strength, yet the system's response exhibits a distinctly nonlinear character. According to our experimental data, the most pronounced strength-gain rate emerges within the initial activation regimes, specifically 0~1 M for NaOH and 0~3% for GGBFS. Beyond these critical thresholds, the incremental improvement diminishes progressively, and the strength evolution tends toward an asymptotic plateau.

This behavior reflects the underlying reaction kinetics. During the initial dissolution stage, the geopolymerization process is highly vigorous, but as reactant availability and diffusion pathways become restricted, the marginal efficiency of additional activator or slag diminishes. Hence, achieving an optimal equilibrium between reagent consumption and mechanical output is essential for maximizing structural efficiency and sustainability.

Equally significant is the interplay between curing duration and chemical composition, which reveals a potent synergistic relationship. Curing time functions not merely as an independent variable, but as a catalytic factor that amplifies the chemical efficacy of alkaline activation and slag integration. Extended curing promotes progressive maturity of the gel network and profound densification of the hardened matrix, an effect that is disproportionately intensified in GGBFS-substituted mixtures.

From a microstructural standpoint, this temporal evolution operates through a dual mechanism: (a) reinforcement of physico-chemical bonding and

cohesion through continuous gel polymerization, and (b) tightening of particle arrangements via enhanced frictional interlocking and volumetric constraint.

Overall, these findings underscore that the development of a high-performance and durable geopolymer system requires the synchronized optimization of activator molarity, precursor composition, and curing regime. Achieving this balance enables efficient utilization of alkaline reagents, enhances long-term structural stability of the matrix, and fosters the formation of a chemically resilient binding network.

Microstructural and elemental analysis of strength development mechanisms

To elucidate the intrinsic mechanisms governing strength development, the microstructural evolution of geopolymer-stabilized specimens was examined through a two-stage SEM–EDS analysis. The first stage focused on the influence of the alkaline activator concentration, specifically the NaOH molarity on morphological transitions within the matrix. As illustrated in Fig. 9, a gradual increase in alkalinity from 1 to 5 M under slag-free conditions induces significant textural reorganization and progressive densification. At low alkalinity (0 M + 0% GGBFS; Fig. 9a), the microstructure displays discrete granular particles weakly bonded through limited interparticle contacts, accompanied by numerous voids and unreacted residues. Such a discontinuous and porous framework can be interpreted as indicative of limited hydroxyl (OH^-) availability, which constrains aluminosilicate

dissolution and suppresses the propagation of a coherent Na-aluminosilicate geopolymeric network. Quantitative ImageJ analysis is in agreement with this trend, revealing a relatively high apparent surface porosity of ≈ 49.8%.

As the NaOH molarity increases from 1 M to 3 and 5 M (in Figs. 9b to 9d, respectively), the matrix undergoes a distinct transformation toward a more compact and well-integrated morphology. This densification is likely associated with the intensified hydrolysis of Si^{4+} and Al^{3+} species under highly alkaline conditions, which facilitates monomer liberation and accelerates polycondensation reactions leading to the formation of cohesive gel phases. Within this consolidated framework, a substantial growth of Na–Al–Si–H gel can be observed and is commonly interpreted as the dominant binding phase that fills residual voids and interconnects adjacent particles. Quantitative ImageJ measurements suggest a consistent densification trend: the apparent surface porosity decreases systematically from approximately 31.1% at 1 M to approximately 30.7% at 3 M and further to approximately 23.3% at 5 M. This consistent reduction in pore volume shows a clear correlation with the significant increase in compressive strength observed macroscopically, a relationship well aligned with previous studies [70, 83]. In summary, these microstructural observations suggest that increasing the degree of alkaline activation enhances both chemical continuity and physical compactness, two synergistic mechanisms that collectively underpin the evolution of strength in geopolymer matrices.

Following the identification of alkalinity as the principal driver of early geopolymerization kinetics, the subsequent analytical stage explored the influence of incorporating GGBFS at varying concentrations (0–9%) under the optimized activation condition of 3 M NaOH. As shown in the SEM micrographs (Fig. 10), a clear and systematic transformation of the matrix morphology occurs with increasing GGBFS content. Compared with the reference specimen (Fig. 10a), which exhibits a flaky, discontinuous texture and limited particle interconnectivity, even a modest addition of 3% GGBFS initiates noticeable matrix consolidation through the generation of compact reaction products. Quantitative ImageJ analysis supports this observation, with an apparent surface porosity of approximately 30.7% for the slag-free sample and 22.1% at 3% GGBFS (Fig. 10b).

To further investigate the chemical characteristics of the stabilized matrix, EDS analysis was conducted on both untreated and geopolymer-treated tailing specimens. Representative EDS spectra of the untreated and treated samples are presented in Fig. 11, while the corresponding elemental compositions are summarized in Table 6. The EDS spectra clearly reveal noticeable variations in elemental distribution after alkali activation and GGBFS incorporation. In particular, the treated specimen exhibited significantly stronger Ca and Si peaks compared with the untreated tailings, indicating the substantial contribution of calcium-rich GGBFS and the enhanced development of geopolymeric reaction products within the stabilized matrix. Quantitative EDS results further confirmed that the Ca

content increased markedly from 3.18 wt% in the untreated tailings to 20.08 wt% in the stabilized specimen. Simultaneously, the Si content increased from 13.85 wt% to 18.06 wt%, while Na was detected in the treated matrix (3.21 wt%) but was absent in the untreated sample, confirming the occurrence of alkali activation reactions.

The coexistence of Ca, Si, Al, and Na within the treated matrix may suggest the formation of calcium–aluminosilicate hydrate and sodium–aluminosilicate hydrate type gels, commonly referred to as C-(A)-S-H and N-A-S-H phases in alkali-activated slag systems. These geopolymeric reaction products are likely responsible for the enhanced particle bonding, progressive filling of interparticle voids, and the development of a denser and more homogeneous microstructure observed in the SEM images. In contrast, the untreated tailings exhibited considerably higher Fe content (36.82 wt%) and lower Ca concentration, reflecting the predominance of unreacted mineral particles prior to stabilization.

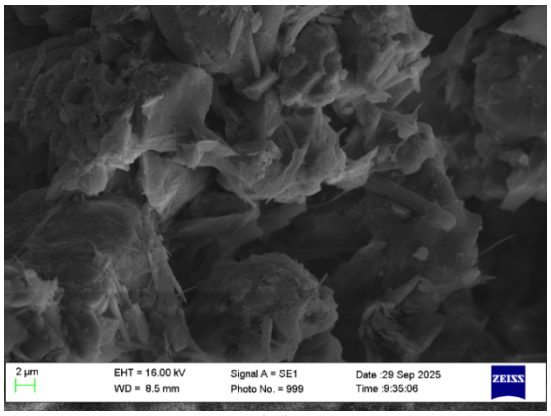

(a)

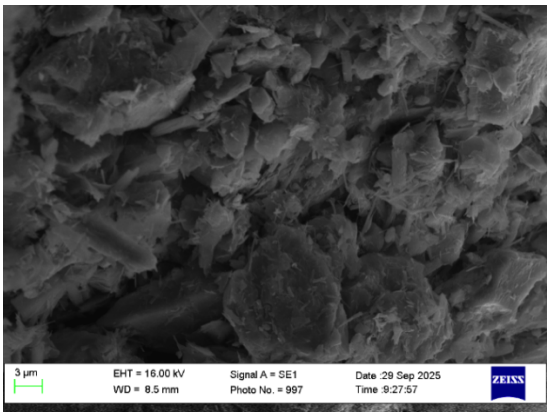

(b)

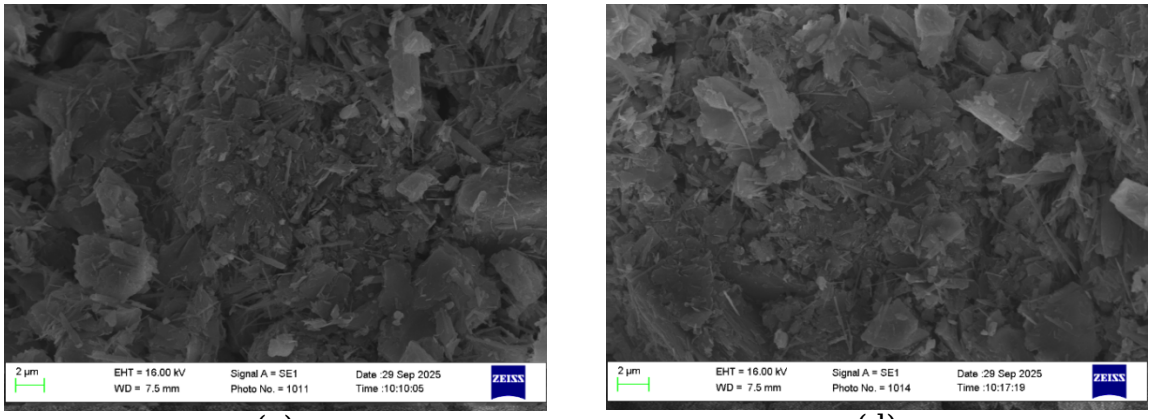

(c) (d)

Figure 9. SEM images of geopolymer improved tailing material: (a) without GGBFS and NaOH; (b) without GGBFS and 1 M NaOH; (c) without GGBFS and 3 M NaOH; (d) without GGBFS and 5 M NaOH

Further incorporation of 6% and 9% GGBFS significantly amplifies this matrix refinement, ultimately producing a relatively uniform and highly compact gel-like matrix characterized by an enhanced cross-linking structure. ImageJ-based quantification indicates a substantial reduction in apparent surface porosity, reaching 5.75% at 6% and approximately 0.81% at 9% GGBFS. These values should be interpreted as indicative of a highly densified structure rather than absolute porosity measurements, while the overall trend clearly reflects the strong influence of calcium-rich slag on matrix consolidation. This progression demonstrates a consistent relationship between microstructural refinement and the observed improvement in macroscopic strength.

(a)

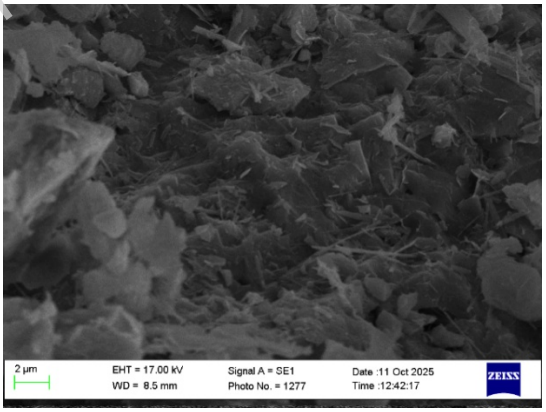

(b)

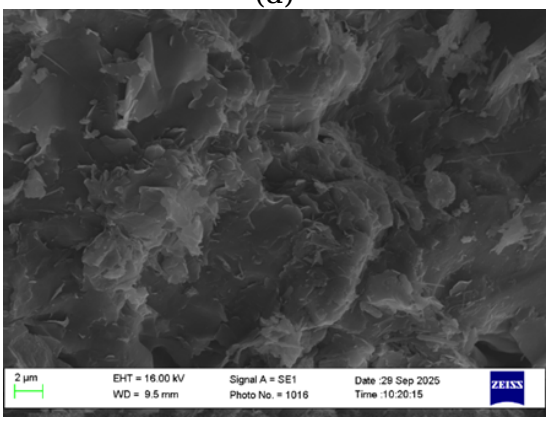

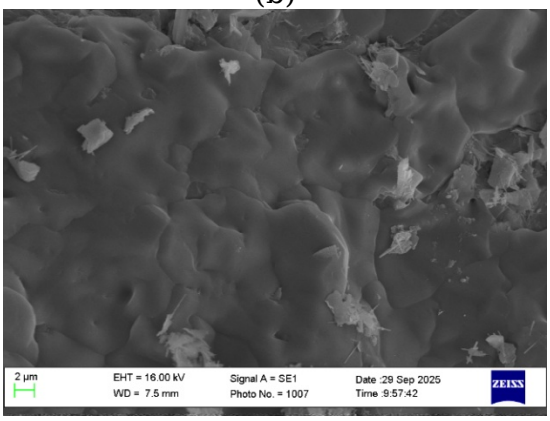

(c) (d)

It should be noted that the ImageJ-based porosity evaluation was derived from two-dimensional SEM images, and therefore represents an apparent surface porosity rather than the true three-dimensional pore structure of the material. Consequently, the reported values should be interpreted qualitatively and mainly used for comparative assessment of microstructural densification among specimens. In addition, although SEM–EDS observations provide useful insights into morphological and elemental variations, the identification of geopolymeric reaction products remains interpretative in the absence of complementary techniques such as XRD or FTIR, which should be investigated through future studies. Overall, the combined SEM and EDS observations suggest that alkali activation and GGBFS incorporation promoted progressive matrix densification and improved interparticle continuity within the tailing material. These microstructural and chemical modifications may have contributed to the enhancement of the mechanical behavior observed in the triaxial tests.

Figure 10. SEM images of geopolymer samples: (a) without GGBFS and 3 M NaOH; (b) with 3% GGBFS and 3 M NaOH; (c) with 6% GGBFS and 3 M NaOH; (d) with 9% GGBFS and 3 M NaOH

Table 6. EDS elemental composition of untreated and geopolymer-treated tailing specimens

Element	Untreated (Wt%)	Treated* (Wt%)
CK	8.7	–
OK	26.23	28.28
NaK	–	3.21
MgK	6.13	5.36
AlK	3.64	4.06

SiK	13.85	18.06
SK	1.44	3.13
CaK	3.18	20.08
FeK	36.82	17.82
Matrix	Correction	Correction

*** Specimen treated with 3 M NaOH and 9% GGBFS.**

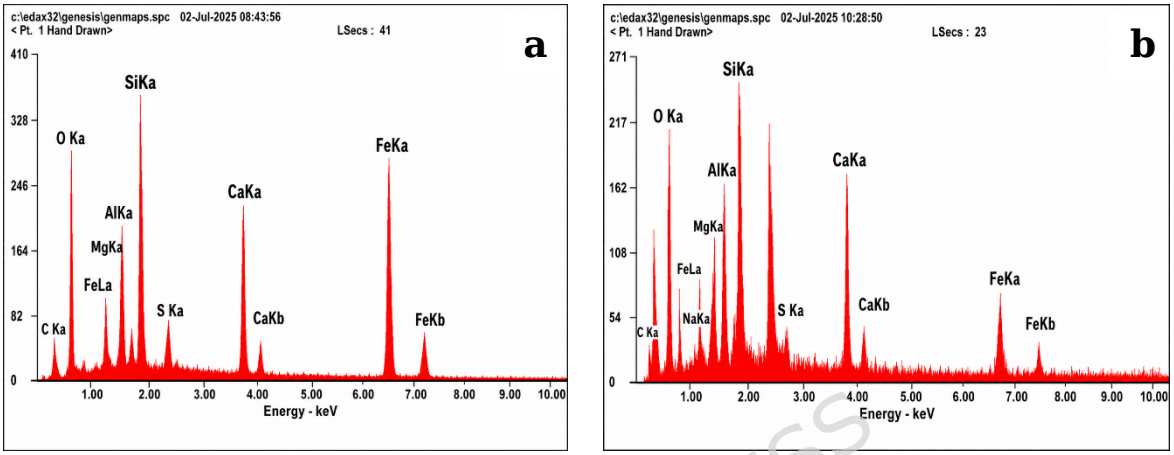

Figure 11. EDS spectra of tailing specimens: (a) untreated, (b) geopolymer-stabilized tailing

The fundamental mechanism underlying this secondary densification involves the formation of a hybrid gel system, wherein calcium-aluminosilicate-hydrate (Ca–Al–Si–H) phases coexist and intergrow with the primary sodium-aluminosilicate-hydrate (Na–Al–Si–H) gel. Calcium ions (Ca^{2+}) released from GGBFS act as charge-balancing species, facilitating cross-link bridging between aluminosilicate chains and thereby enhancing structural integrity [84, 85]. As highlighted by Wang and Cao (2023), an elevated Ca/Si ratio promotes the development of a denser and more cohesive gel framework. The resulting dual-gel architecture, commonly denoted as Ca–(Na)–Al–Si–H, not only fills residual capillary voids but also immobilizes unreacted particles and strengthens the binder's overall continuity. Consequently, these microstructural refinements culminate in a substantial reduction in porosity

and a pronounced improvement in cohesion and compressive strength, in agreement with previous findings [20].

Moreover, studies have shown that in iron-rich tailings, NaOH alters the role of iron from an inert phase to a semi-active structural component, enabling Fe to be incorporated into the gel network. This process leads to the formation of Na–Al/Fe–Si–H and Ca–(Al/Fe)–Si–H gels, which exhibit higher elastic moduli and reduced crack susceptibility, thereby enhancing the mechanical integrity of the stabilized matrix [86]. In addition, the observed improvement in mechanical strength can partly be attributed to a reduction in the surface free energy of the particles in the presence of NaOH. This effect increases the tendency for interparticle interaction, interlocking, and densification, ultimately leading to a reduction in effective porosity and improved mechanical stability [87].

Evaluation of consolidation characteristics and swelling potential

The consolidation response of geopolymer-stabilized tailings was examined to investigate how alkaline activation modulates compressibility reduction and enhances volumetric stability. This evaluation was based on one-dimensional consolidation data, focusing on the compression index (Cc) and swell index (Cs) derived from e–log(σ′) relationships. As summarized in Table 7, both indices exhibit a distinct and systematic decline with increasing NaOH molarity and GGBFS dosage.

Table 7. Compressibility and Swelling Indices of the Tested Series

Series	Compression Index	Swelling Index

Base	0.651	0.032
1 M	0.354	0.023
3 M	0.338	0.022
5 M	0.281	0.017
3 M + 3% GGBFS	0.145	0.012
3 M + 6% GGBFS	0.129	0.010
3 M + 9% GGBFS	0.032	0.007

The untreated control sample demonstrated pronounced compressibility (Cc=0.651), indicating a loosely packed skeletal structure with a high void ratio and limited resistance to deformation under loading. Similarly, a Cs value of 0.032 reflected moderate swelling potential, typical of fine-grained IOT with limited intrinsic cementitious bonding.

Progressive alkaline activation using NaOH substantially enhanced matrix rigidity and volumetric integrity. Increasing activator molarity from 1 M to 5 M reduced Cc from 0.354 to 0.281, a 57% decrease relative to the untreated baseline. This improvement in compressibility resistance is attributed to the formation of cohesive Na–Al–Si–H gel networks, which establish robust interparticle cementation bridges and reinforce the tailings framework [88]. The simultaneous reduction in Cs to approximately 0.017 further suggests enhanced stability of the geopolymeric matrix and reduced elastic rebound during unloading.

Incorporation of calcium-rich GGBFS under constant 3 M NaOH activation produced a distinctive, nonlinear improvement in consolidation characteristics. Moderate slag additions of 3% and 6% reduced Cc to

approximately 0.145 and 0.129, respectively. In comparison, the 9% GGBFS mixture achieved an optimal Cc of 0.032, representing a 95% reduction compared with untreated tailings and a 90% reduction relative to slag-free geopolymers. This substantial attenuation of compressibility indicates a significant modification in the material's mechanical structure.

Synergistic reactions among NaOH, tailings aluminosilicates, and GGBFS facilitate concurrent precipitation of Ca–Al–Si–H and Na–Al–Si–H gels, which progressively fill residual pore spaces and yield a densely bonded load-bearing matrix. SEM observations further confirmed this behavior by revealing a highly compact and continuous microstructure with extensive particle bonding and significant pore refinement in the stabilized specimens, particularly in the 9% GGBFS mixture. The resulting specimens, with Cc ≈ 0.032 and Cs ≈ 0.007 (for 3 M + 9% GGBFS), display consolidation characteristics comparable to rock-like or heavily over-consolidated clays.

From a geotechnical standpoint, this behavior reflects the emergence of a “pseudo-preconsolidation stress” generated by chemical cementation. Accordingly, the coexistence of very low compressibility and relatively high shear strength is considered mechanically consistent, since both responses originate from the same densified and strongly cemented geopolymeric framework. Accordingly, the optimized formulation (9% GGBFS + 3 M NaOH) virtually eliminates the potential for primary consolidation settlement under conventional structural loading, positioning it as a sustainable and high-performance stabilization strategy for saturated low-plasticity soils [89-91].

Evaluation of chemical stability and heavy metal immobilization efficiency

To comprehensively assess the environmental robustness and chemical durability of the developed geopolymeric matrix, the TCLP was employed to quantify the immobilization efficiency of heavy metal contaminants achieved through NaOH–GGBFS activation. The results, illustrated in Fig. 12, demonstrate a marked suppression of heavy metal leaching, particularly Ni, Cu, Zn, Pb, and Ba attributable to the formation of a densely cross-linked geopolymeric network whose stability far exceeds U.S. EPA regulatory thresholds. Figure 12a depicts the effect of NaOH molarity, whereas Fig. 12b presents the corresponding variations induced by incremental GGBFS replacement under constant 3 M NaOH activation. Collectively, these findings confirm the efficacy of the stabilization/solidification process, driven by synergistic physical encapsulation and chemical fixation mechanisms operating within the dual gel phases [67]. A closer examination reveals cooperative strengthening effects between the two activating components. Increasing NaOH concentration from 1 M to 5 M progressively densified the matrix and reduced permeability, thereby lowering Pb leachate concentrations from 2.10 mg/L to 0.20 mg/L. In contrast, the incorporation of GGBFS exerted an even more substantial influence.

Within this coherent microstructure, the restriction of fluid migration pathways and the formation of strong ionic and covalent bonds between metal species and the aluminosilicate framework provide the primary mechanism

for chemical immobilization. Consequently, leachate metal concentrations reached their lowest measured values, with Pb at 0.018 mg/L, Ni at approximately 0.10 mg/L, and Zn at approximately 0.12 mg/L, corresponding to immobilization efficiencies exceeding 90%. The results of present study are in agreement with those reported by Maqbool et al., confirming the effectiveness of aluminosilicate-based geopolymeric matrices in heavy metal immobilization. The consistency among mechanical, microstructural, and geochemical evidence confirms the decisive role of 9% slag in simultaneously enhancing the mechanical stability and environmental safety.

Each metal species exhibited distinct stabilization pathways within the highly alkaline geopolymer environment. Nickel (Ni) and Zinc (Zn) were primarily immobilized via the precipitation of insoluble hydroxides and carbonates, i.e. $Ni(OH)_2$, $Zn(OH)_2$ and $ZnCO_3$. Copper (Cu) transformed into the thermodynamically stable oxide phase (CuO), while Barium (Ba) was sequestered through the formation of sparingly soluble barium sulfate ($BaSO_4$). Lead (Pb), beyond precipitation as $PbCO_3$, was partially incorporated into the Ca–Al–Si–H gel structure via ionic substitution, explaining its exceptionally low leachability. These immobilization routes align closely with recently reported mechanisms for mineral-waste-based geopolymers [92, 93].

For comparative benchmarking, the present results were evaluated against those of Pahlavan et al., who enhanced geopolymer performance using algal biochar as an additive. Their 5% biochar-reinforced matrix achieved an

approximately 80% removal efficiency for Cu^{2+} and Zn^{2+}, primarily through surface adsorption on biochar functional groups [94]. However, the NaOH–GGBFS system reported herein achieved greater than 90% immobilization for all target metals, demonstrating actual structural incorporation within Ca–Al–Si–H gels rather than mere surface sorption. The exceptional compactness and calcium-rich reactive sites provided by GGBFS thus enable a deeper level of chemical stabilization compared with adsorption-based systems.

Accordingly, the NaOH–GGBFS geopolymer emerges as a low-carbon, environmentally sustainable technology for managing mine tailings, offering a chemically durable containment medium with minimal leachability and long-term ecological safety.

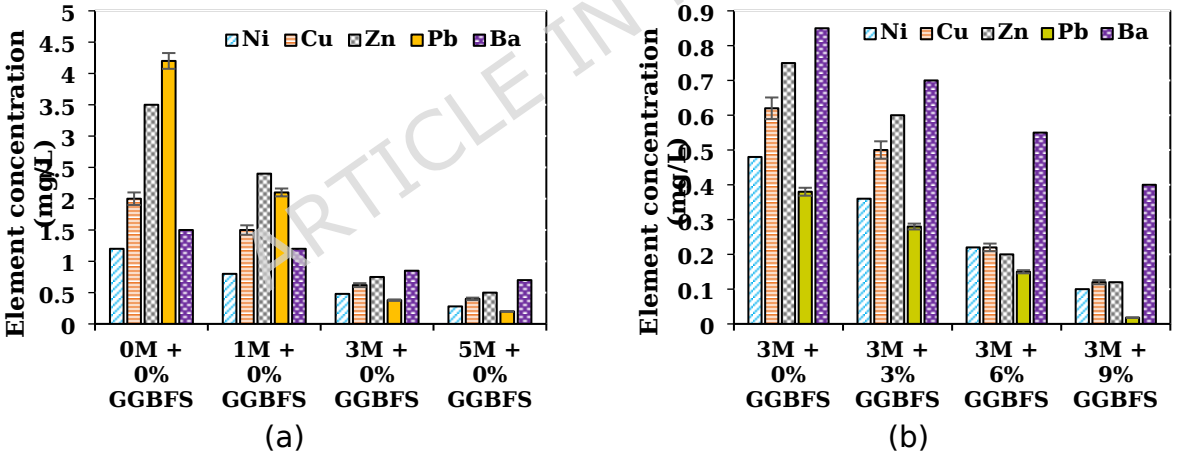

Figure 12. Variation of metal concentrations in the reference and stabilized samples: (a) effect of NaOH molarity, and (b) effect of different GGBFS contents at a fixed 3 M NaOH concentration

Life cycle assessment

To deliver a comprehensive perspective on sustainability and quantify the environmental footprint of the proposed stabilization technology, a cradle-to-gate LCA was conducted [95], comparing the optimized NaOH–GGBFS

system with the conventional OPC-based methodology. As illustrated in Fig. 13, the LCA outcomes unequivocally demonstrate the superior ecological performance of the geopolymer mixtures across all major impact categories. The most notable achievement of the geopolymer formulation lies in its 30–35% reduction in GWP and a comparable 30% decrease in fossil-fuel consumption relative to OPC-based specimens. This substantial mitigation arises directly from the complete elimination of OPC production, which has long been recognized as a significant industrial source of CO_2 emissions. In addition, the geopolymer system yields extended environmental co-benefits, including a 15–20% reduction in suspended particles below 2.5 μm ($PM_{2.5}$) emissions and land-resource occupation [96], thereby reinforcing its alignment with contemporary decarbonization trajectories within the construction sector [25, 97, 98].

However, the comprehensive environmental profile also highlights a minor trade-off. The human toxicity potential (HTP) of geopolymer specimens was found to be approximately 10–20% higher than that of the cementitious controls, primarily due to the energy-intensive industrial synthesis of NaOH, a recognized bottleneck in the large-scale commercialization of alkaline activators [99]. Nevertheless, the incorporation of GGBFS, an industrial by-product, partially offsets this drawback by valorizing waste materials and enhancing the system's overall eco-efficiency [100].

Overall, the net environmental advantages of the geopolymer system substantially outweigh its minor drawbacks. The observed 30–35% reduction

in carbon footprint constitutes a significant advancement toward achieving the United Nations sustainable development goals [101]. Technically, although OPC-treated specimens exhibit marginally higher mechanical strength, the geopolymer formulations deliver structurally reliable and functionally adequate performance for tailings stabilization and light civil infrastructure applications, which is in agreement with the work of Manaviparast et al [95]. Importantly, the geopolymer mixtures developed in this study satisfy the minimum mechanical performance requirements for the intended application, while OPC-based systems reported in the literature for similar applications are designed to achieve comparable performance levels. In this context, environmental impacts are interpreted in relation to the achieved engineering performance, allowing for a consistent comparison between alternative stabilization systems, as commonly adopted in previous studies.

Therefore, this study confirms that alkali-activated geopolymers represent a low-carbon, environmentally responsible, and sustainable alternative to Portland cement for the management of mineral waste and ground improvement in engineering contexts. Therefore, the comparison in the LCA is carried out on a functional basis, assuming that both systems fulfill the minimum mechanical performance necessary for the intended use.

Moreover, the findings of this study are consistent with a broader corpus of research emphasizing the potential of alkali-activated mine tailings and similar mining wastes as low-carbon, value-added construction materials

within a circular economy framework [102]. Extensive reviews indicate that alkali activation can convert large volumes of mine tailings, typically considered waste and associated with long-term environmental risks into solid, concrete-like materials by leveraging their inherent aluminosilicate content [3]. This transformation not only reduces dependence on virgin raw materials but also stabilizes hazardous constituents within the waste matrix. Further studies report that alkali-activated binders derived from mining wastes, or their blends with industrial by-products, can achieve favorable mechanical performance and reduced CO_2 emissions compared with conventional cementitious systems, while effectively addressing large-scale waste streams through stabilization and valorization pathways [103]. Such valorization strategies are fully consistent with life cycle thinking, as they not only minimize environmental impacts and reduce greenhouse gas emissions relative to OPC-based materials, but also repurpose mine tailings as sustainable raw resources, thereby contributing to resource conservation and lowering the material footprint in construction applications [104].

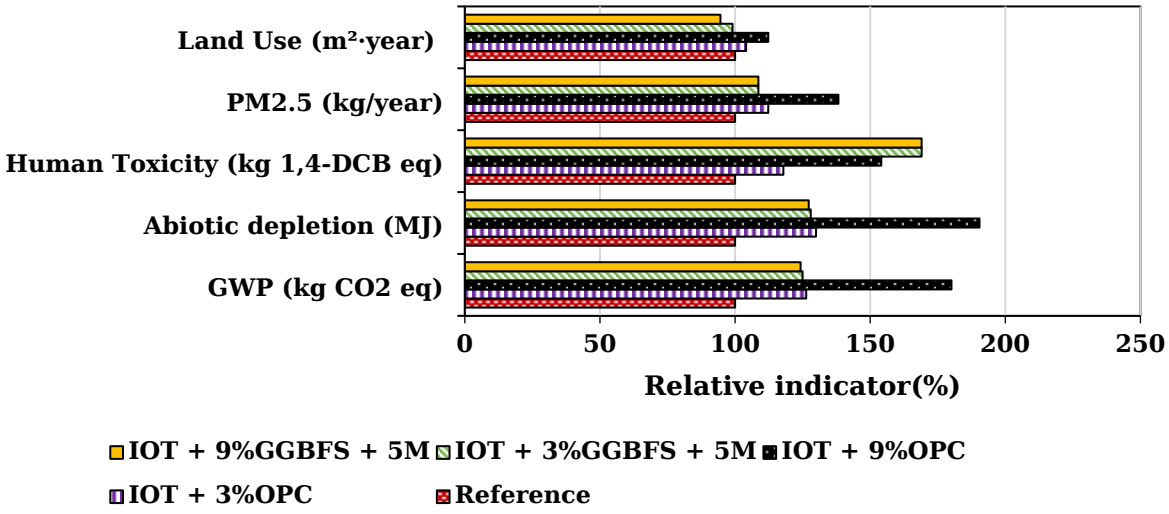

Figure 13. Environmental impact assessment of different mix designs

Conclusion

This study presents a novel, multi-scale approach for transforming IOTs into durable and environmentally safe geotechnical materials through alkali activation with a hybrid NaOH–GGBFS geopolymer binder. Integrating mechanical, microstructural, and environmental evaluations, the results highlight alkali-activated tailings as a low-carbon, high-performance alternative for sustainable ground improvement and hazardous material management.

Based on the results, Optimization of NaOH molarity and slag content significantly enhanced mechanical properties, with undrained shear strength exceeding 5.8 MPa and marked increase in cohesion and friction angle. The mechanical improvement can be attributed to the formation of a dense geopolymeric matrix of N–A–S–H and C–A–S–H gels, promoting particle bonding, refined microstructure, and improved stress transfer. Moreover, heavy metal leaching was effectively stabilized, with reductions exceeding

90%. Also, LCA indicated up to 35% reduction in global warming potential and fossil energy demand compared to Portland cement-based systems. However, the limitations include controlled laboratory conditions, lack of long-term field performance evaluation, limited environmental exposure testing, and SEM–EDS-based microstructural analysis that may not fully capture 3D structure of the material. Future research should include unsaturated soil testing, advanced microstructural characterization, long-term durability assessment, field validation, and broader mix-design optimization.

Data Availability Statement

All data used in this study have been included in the manuscript.

Declaration of Competing Interest

The authors declare that they have no known competing financial interests or personal relationships that could have influenced the results of the study reported in this paper.

Funding

The authors declare no financial support for the current study.

References

[1] X. Cui, Y. Geng, T. Li, R. Zhao, X. Li, and Z. Cui, "Field application and effect evaluation of different iron tailings soil utilization technologies," *Resources, Conservation and Recycling,* vol. 173, p. 105746, 2021/10/01/ 2021, doi: https://doi.org/10.1016/j.resconrec.2021.105746.

[2] X. Zhan, L. Tang, Z. Yue, H. Lu, and J. Wang, "Enhanced mechanical properties and mechanism of iron ore tailings-based geopolymers modified by municipal solid waste incineration fly ash," *Journal of Building Engineering,* vol. 98, p. 111456, 2024.

[3] J. Kiventerä, P. Perumal, J. Yliniemi, and M. Illikainen, "Mine tailings as

a raw material in alkali activation: A review," *International Journal of Minerals, Metallurgy and Materials,* vol. 27, no. 8, pp. 1009-1020, 2020.
[4] S. Kalisz, K. Kibort, J. Mioduska, M. Lieder, and A. Małachowska, "Waste management in the mining industry of metals ores, coal, oil and natural gas-A review," *Journal of environmental management,* vol. 304, p. 114239, 2022.
[5] N. C. Consoli, L. F. Tomasi, and S. F. Veloso Marques, "Cement-enhancing mechanical behavior of tailings behind upstream tailings dam for safe decommissioning," *Journal of Materials in Civil Engineering,* vol. 35, no. 5, p. 06023001, 2023.
[6] S. Ghasemi, A. Behnamfard, and R. Arjmand, "Iron ore tailings valorization through separate characterization and upgradation of different tailings streams of an Iranian iron ore processing plant," *Environmental Science and Pollution Research,* vol. 30, no. 54, pp. 115448-115460, 2023.
[7] N. C. Consoli, A. P. da Silva, H. P. Nierwinski, and J. Sosnoski, "Durability, strength, and stiffness of compacted gold tailings–cement mixes," *Canadian Geotechnical Journal,* vol. 55, no. 4, pp. 486-494, 2018.
[8] D. B. Mazzinghy, R. A. Figueiredo, A. Parbhakar-Fox, M. Yahyaei, J. Vaughan, and M. S. Powell, "Trialling one-part geopolymer production including iron ore tailings as fillers," *International Journal of Mining, Reclamation and Environment,* vol. 36, no. 5, pp. 356-367, 2022.
[9] Y. H. M. Amran, R. Alyousef, H. Alabduljabbar, and M. El-Zeadani, "Clean production and properties of geopolymer concrete; A review," *Journal of Cleaner Production,* vol. 251, p. 119679, 2020/04/01/ 2020, doi: https://doi.org/10.1016/j.jclepro.2019.119679.
[10] R. Chaudhury, U. Sharma, P. Thapliyal, and L. Singh, "Low-CO2 emission strategies to achieve net zero target in cement sector," *Journal of Cleaner Production,* p. 137466, 2023.
[11] J. Khatib, *Sustainability of construction materials*. Woodhead Publishing, 2016.
[12] R. Asghar, M. A. Khan, R. Alyousef, M. F. Javed, and M. Ali, "Promoting the green Construction: Scientometric review on the mechanical and structural performance of geopolymer concrete," *Construction and Building Materials,* vol. 368, p. 130502, 2023/03/03/ 2023, doi: https://doi.org/10.1016/j.conbuildmat.2023.130502.
[13] E. Abuowda, H. El-Hassan, and T. El-Maaddawy, "Characterization of geopolymer masonry mortars incorporating recycled fine aggregates," *Sustainability,* vol. 16, no. 18, p. 8147, 2024.
[14] S. Gupta and S. Kumar, "Mechanical and microstructural analysis of soft kaolin clay stabilized by GGBS and dolomite-based geopolymer," *Construction and Building Materials,* vol. 421, p. 135702, 2024.
[15] O. Chakkor, "Durability and Microstructural Evaluation of Geopolymer Mortars Exposed to Sulphuric Acid Using Industrial By-Product

Fillers," *Polymers,* vol. 17, no. 17, p. 2310, 2025.
[16] Z. Feng *et al.*, "Recent advances in tailings waste as geopolymers for construction: Current challenges and prospects," *Minerals Engineering,* vol. 230, p. 109439, 2025.
[17] Z. Gao, Y. Li, H. Qian, and M. Wei, "Environmental, economic, and social sustainability assessment: A case of using contaminated tailings stabilized by waste-based geopolymer as road base," *Science of The Total Environment,* vol. 888, p. 164092, 2023/08/25/ 2023, doi: https://doi.org/10.1016/j.scitotenv.2023.164092.
[18] A. Alsalman, L. N. Assi, R. S. Kareem, K. Carter, and P. Ziehl, "Energy and CO2 emission assessments of alkali-activated concrete and Ordinary Portland Cement concrete: A comparative analysis of different grades of concrete," *Cleaner Environmental Systems,* vol. 3, p. 100047, 2021/12/01/ 2021, doi: https://doi.org/10.1016/j.cesys.2021.100047.
[19] J. Kiventerä, I. Lancellotti, M. Catauro, F. Dal Poggetto, C. Leonelli, and M. Illikainen, "Alkali activation as new option for gold mine tailings inertization," *Journal of cleaner production,* vol. 187, pp. 76-84, 2018.
[20] N. Cristelo, J. Coelho, M. Oliveira, N. Cesar Consoli, Á. Palomo, and A. Fernández-Jiménez, "Recycling and application of mine tailings in alkali-activated cements and mortars—strength development and environmental assessment," *Applied Sciences,* vol. 10, no. 6, p. 2084, 2020.
[21] Z. Pan, C. Zhang, Y. Li, and C. Yang, "Solidification/stabilization of gold ore tailings powder using sustainable waste-based composite geopolymer," *Engineering Geology,* vol. 309, p. 106793, 2022/11/01/ 2022, doi: https://doi.org/10.1016/j.enggeo.2022.106793.
[22] J. Yao, H. Qiu, H. He, X. Chen, and G. Hao, "Application of a soft soil stabilized by composite geopolymer," *Journal of Performance of Constructed Facilities,* vol. 35, no. 4, p. 04021018, 2021.
[23] B. C. McLellan, R. P. Williams, J. Lay, A. Van Riessen, and G. D. Corder, "Costs and carbon emissions for geopolymer pastes in comparison to ordinary portland cement," *Journal of cleaner production,* vol. 19, no. 9-10, pp. 1080-1090, 2011.
[24] S. Hanjitsuwan, S. Hunpratub, P. Thongbai, S. Maensiri, V. Sata, and P. Chindaprasirt, "Effects of NaOH concentrations on physical and electrical properties of high calcium fly ash geopolymer paste," *Cement and concrete composites,* vol. 45, pp. 9-14, 2014.
[25] Y. Li *et al.*, "Environmental impact analysis of blast furnace slag applied to ordinary Portland cement production," *Journal of Cleaner Production,* vol. 120, pp. 221-230, 2016/05/01/ 2016, doi: https://doi.org/10.1016/j.jclepro.2015.12.071.
[26] G. Görhan, R. Aslaner, and O. Şinik, "The effect of curing on the properties of metakaolin and fly ash-based geopolymer paste," *Composites Part B: Engineering,* vol. 97, pp. 329-335, 2016.
[27] B. Lee, G. Kim, R. Kim, B. Cho, S. Lee, and C.-M. Chon, "Strength

development properties of geopolymer paste and mortar with respect to amorphous Si/Al ratio of fly ash," *Construction and Building Materials,* vol. 151, pp. 512-519, 2017.
[28] D. A. Salas, A. D. Ramirez, N. Ulloa, H. Baykara, and A. J. Boero, "Life cycle assessment of geopolymer concrete," *Construction and Building Materials,* vol. 190, pp. 170-177, 2018/11/30/ 2018, doi: https://doi.org/10.1016/j.conbuildmat.2018.09.123.
[29] Q. Sun *et al.*, "Preparation and microstructure of fly ash geopolymer paste backfill material," *Journal of Cleaner Production,* vol. 225, pp. 376-390, 2019.
[30] N. S. D. M. Azhar, F. F. Zainal, and M. M. A. B. Abdullah, "A review on durability performance of reinforcement bar in geopolymer paste compare with its performance in ordinary Portland cement paste," in *AIP Conference Proceedings*, 2019, vol. 2129, no. 1: AIP Publishing LLC, p. 020046.
[31] M. G. Khalil, F. Elgabbas, M. S. El-Feky, and H. El-Shafie, "Performance of geopolymer mortar cured under ambient temperature," *Construction and Building Materials,* vol. 242, p. 118090, 2020.
[32] F. Kantarci, İ. Türkmen, and E. Ekinci, "Influence of various factors on properties of geopolymer paste: A comparative study," *Structural Concrete,* vol. 22, pp. E315-E331, 2021.
[33] M. Sitarz, I. Hager, and M. Choińska, "Evolution of mechanical properties with time of fly-ash-based geopolymer mortars under the effect of granulated ground blast furnace slag addition," *Energies,* vol. 13, no. 5, p. 1135, 2020.
[34] T. Chen, B. Ren, Z. Wang, X. Meng, Y. Ning, and Y. Lv, "Effect of early strength agent on the hydration of geopolymer mortar at low temperatures," *Case Studies in Construction Materials,* vol. 17, p. e01419, 2022.
[35] A. Agnihotri and P. Ramana, "GGBS: Fly-Ash evaluation and mechanical properties within high strength concrete," *Materials Today: Proceedings,* vol. 50, pp. 2404-2410, 2022.
[36] V. Benavent, H. Lahalle, C. Patapy, G. Renaudin, and M. Cyr, "Microstructural evolution of a sodium metakaolin-based geopolymer paste in neutral and CEM V basic environment," *Cement and Concrete Research,* vol. 161, p. 106897, 2022.
[37] A. E. Alexander and A. Shashikala, "Studies on the microstructure and durability characteristics of ambient cured FA-GGBS based geopolymer mortar," *Construction and Building Materials,* vol. 347, p. 128538, 2022.
[38] A. Tamilarasan and O. Suganya, "Effect of varying molarity and curing conditions on the mechanical and microstructural characteristics of alkali activated GGBS binder," *Materials Research Express,* vol. 10, no. 9, p. 095305, 2023.
[39] Q. Maqbool, Mobili, A., Blasi, E., Sabbatini, S., Ruello, M. L., &

Tittarelli, F, "Sustainable alkali activated mortars for the immobilization of heavy metals from copper mine tailings," *ACS Sustainable Resource Management,* vol. 1(1), pp. 154–164, 2024, doi: https://doi.org/10.1021/acssusresmgt.3c00002

[40] G. Huang, Wang, M., Liu, Q., Zhao, S., Liu, H., Liu, F., Feng, L., & Song, J, "Simultaneous utilization of mine tailings and steel slag for producing geopolymers: Alkali hydrothermal activation, workability, strength, and hydration mechanism," *Construction and Building Materials,* vol. 414, p. 135029, 2024, doi: https://doi.org/10.1016/j.conbuildmat.2024.135029

[41] H. Zou, W. Zhong, X. Zhao, and L. Fan, "Optimizing geopolymer mortar for shotcrete applications by focusing on flowability and early-age mechanical characteristics," *Construction and Building Materials,* vol. 418, p. 135290, 2024.

[42] M. Ziada, H. Tanyildizi, and M. Uysal, "The influence of carbon nanotube on underwater geopolymer paste based on metakaolin and slag," *Construction and Building Materials,* vol. 414, p. 135047, 2024.

[43] J. Fu, Y.-g. Chen, J.-h. He, and H. Zhou, "Solidification/stabilization of composite heavy metals using red mud-blast furnace slag based geopolymer," *Environmental Earth Sciences,* vol. 83, no. 18, p. 533, 2024.

[44] Y. Min, J. Wu, B. Li, M. Zhang, and J. Zhang, "Physicochemical and mechanical behavior of the one-part geopolymer paste exposed to hydrochloric and sulfuric acids," *Journal of Materials in Civil Engineering,* vol. 35, no. 3, p. 04022456, 2023.

[45] Y. Zhang, Liu, H., & Wang, J, "Effect of alkali activator and granulated blast furnace slag on the properties of lithium slag based high strength lightweight aggregates," *Scientific Reports,* vol. 15, p. 16048, 2025, doi: https://www.nature.com/articles/s41598-025-16048-8.

[46] R. Fernández *et al.*, "Comparative Assessment of Cement and Geopolymer Immobilization Approaches: Short-Term Leaching Performance of Thermally Treated Ion Exchange Resin Waste Forms," *Applied Sciences,* vol. 15, no. 20, p. 11196, 2025.

[47] Z. Abeoub, S. Djaknoun, M. Saïdani, R. S. Amrouche, E. Ouedraogo, and M. Trari, "Journal of the mechanical behavior of materials: An experimental approach for the determination of the physical and mechanical properties of a sustainable geopolymer mortar made with Algerian ground-granulated blast furnace slag," 2025.

[48] S. S. N. N. Simon A, "Reaction Products, Microstructure, and Leaching Potential

of Alkali-Activated Mine Tailings–Slag Binders," *Journal of Materials in Civil Engineering,* vol. 38(1), no. 0899-1561, p. 04025503, 2026, doi: https://doi.org/10.1061/JMCEE7.MTENG-20621.

[49] A. D854, "Standard Test Methods for Specific Gravity of Soil Solids by

Water

Pycnometer," ASTM 2006, West Conshohocken, Pa. (2006).
[50] D.-. ASTM, "Standard test methods for liquid limit, plastic limit, and plasticity index of soils," *D4318-10,* 2010.
[51] D.-. ASTM, "Standard test method for shrinkage

factors of soils by the water submersion method," *ASTM*

International, West Conshohocken, 2024.
[52] A. D2487-17, "Standard Practice for Classification of Soils for Engineering Purposes (Unified Soil Classification System)," *ASTM International, West Conshohocken, PA, USA,* vol. Volume 4, pp. pp. 249–260, 2017.
[53] A. D698-12, "Standard test methods for laboratory compaction

characteristics of soil using standard effort (12 400 ft-lbf/ft3 (600 kN-m/

m3))," vol. West Conshohocken, PA: ASTM International, 2012.
[54] N. C. Consoli *et al.*, "Effect of cement type on compacted iron ore tailings-binder response blends: comparative study," *Journal of Materials in Civil Engineering,* vol. 36, no. 8, p. 04024230, 2024.
[55] P. Chauhan, A. El Hajjar, N. Prime, and O. Plé, "Unsaturated behavior of rammed earth: Experimentation towards numerical modelling," *Construction and Building Materials,* vol. 227, p. 116646, 2019/12/10/ 2019, doi: https://doi.org/10.1016/j.conbuildmat.2019.08.027.
[56] Y. Wang, P. Guo, X. Li, H. Lin, Y. Liu, and H. Yuan, "Behavior of fiber-reinforced and lime-stabilized clayey soil in triaxial tests," *Applied Sciences,* vol. 9, no. 5, p. 900, 2019.
[57] T. V. Duong *et al.*, "Effects of water and fines contents on the resilient modulus of the interlayer soil of railway substructure," *Acta Geotechnica,* vol. 11, no. 1, pp. 51-59, 2016.
[58] J. Muñoz-Castelblanco, P. Delage, J.-M. Pereira, and Y.-J. Cui, "On-sample water content measurement for a complete local monitoring in triaxial testing of unsaturated soils," *Géotechnique,* vol. 62, no. 7, pp. 595-604, 2012.
[59] U.S.EPA, "1311.pdf," Accessed March 27, 2023, doi: https://www.epa.gov/sites/default/files/2015-12/documents/1311.pdf.
[60] N. Shariatmadari, H. Hasanzadehshooiili, P. Ghadir, F. Saeidi, and F. Moharami, "Compressive strength of sandy soils stabilized with alkali-activated volcanic ash and slag," *Journal of Materials in Civil Engineering,* vol. 33, no. 11, p. 04021295, 2021.
[61] ASTM D 4972–01, "Standard test method for pH of soils," *ASTM International, West Conshohocken, PA, USA,* 2007.
[62] M. Shakil, S. Nazar, H. F. M. Ameen, A. Shahzad, and F. Ahmad, "A comparative study of ground granulated blast furnace slag and bagasse ash incorporation on enhancing mechanical properties of

expansive soil," *Results in Engineering,* vol. 25, p. 103569, 2025/03/01/ 2025, doi: https://doi.org/10.1016/j.rineng.2024.103569.
[63] D. Debnath and S. Kumar Chouksey, "Experimental study of strength behavior of soft soil stabilised with alkali activated copper slag," *Materials Today: Proceedings,* vol. 65, pp. 2112-2117, 2022/01/01/ 2022, doi: https://doi.org/10.1016/j.matpr.2022.07.106.
[64] J. Kiventerä, L. Golek, J. Yliniemi, V. Ferreira, J. Deja, and M. Illikainen, "Utilization of sulphidic tailings from gold mine as a raw material in geopolymerization," *International Journal of Mineral Processing,* vol. 149, pp. 104-110, 2016.
[65] H. Amjad, E.-S. Abd-Elaal, X. Ma, T. Benn, and M. Fisher, "A Critical Review of Iron Ore Tailings as Cement and Aggregate Substitutes for Robust Infrastructure: Mechanical, Durability, and Socio-Economic Impacts," *Journal of Cleaner Production,* p. 144853, 2025.
[66] M. Sun, Y. Fu, W. Wang, Y. Yang, and A. Wang, "Experimental research on the compression property of geopolymer concrete with molybdenum tailings as a building material," *Buildings,* vol. 12, no. 10, p. 1596, 2022.
[67] X. Ji, X. Gu, Z. Wang, S. Xu, H. Jiang, and E. Yilmaz, "Admixture effects on the rheological/mechanical behavior and micro-structure evolution of alkali-activated slag backfills," *Minerals,* vol. 13, no. 1, p. 30, 2022.
[68] B. Bagriacik, "Utilization of alkali-activated construction demolition waste for sandy soil improvement with large-scale laboratory experiments," *Construction and Building Materials,* vol. 302, p. 124173, 2021/10/04/ 2021, doi: https://doi.org/10.1016/j.conbuildmat.2021.124173.
[69] Ü. Yurt and H. Bayraktar, "Towards innovative and sustainable building materials: Effect of alkali activator concentration on the performance of waste brick powder-based geopolymer composites," *Environmental Research,* vol. 283, p. 122109, 2025/10/15/ 2025, doi: https://doi.org/10.1016/j.envres.2025.122109.
[70] E. Poojalakshmi, P. Nagarajan, J. Sudhakumar, and B. S. Thomas, "Impact of alkaline activator concentration on mechanical properties and microstructure of a ternary blended one-part geopolymer cement," *Scientific Reports,* vol. 15, no. 1, p. 33808, 2025.
[71] L. Reig, L. Soriano, M. V. Borrachero, J. Monzó, and J. Payá, "Influence of the activator concentration and calcium hydroxide addition on the properties of alkali-activated porcelain stoneware," *Construction and Building Materials,* vol. 63, pp. 214-222, 2014/07/30/ 2014, doi: https://doi.org/10.1016/j.conbuildmat.2014.04.023.
[72] M. Verma and N. Dev, "Effect of ground granulated blast furnace slag and fly ash ratio and the curing conditions on the mechanical properties of geopolymer concrete," *Structural concrete,* vol. 23, no. 4, pp. 2015-2029, 2022.
[73] S. Kara, S. Erdem, and R. A. G. Lezcano, "MgO-based cementitious composites for sustainable and energy efficient building design,"

Sustainability, vol. 13, no. 16, p. 9188, 2021.
[74] S. Shrestha and P. K. Kolay, "Strength, durability and microstructural properties of fly ash-ground granulated blast furnace slag based geopolymer stabilized high plastic clay," *Transportation Geotechnics,* vol. 56, p. 101770, 2026/01/01/ 2026, doi: https://doi.org/10.1016/j.trgeo.2025.101770.
[75] T. A. Wassie, G. Demir, and U. Köktan, "Influence of Curing Time and Initial Moisture Content on Metakaolin-Based Geopolymer-Stabilized Soft Soil," *Advances in Civil Engineering,* vol. 2023, no. 1, p. 6673716, 2023.
[76] A. Isik, "Experimental study on compressive strength of clay soil stabilized with construction and demolition waste-based geopolymer," *Bulletin of Engineering Geology and the Environment,* vol. 84, no. 7, p. 380, 2025.
[77] M. Chen, D. Wu, K. Chen, P. Cheng, and Y. Tang, "The influence of fly ash-based geopolymer on the mechanical properties of OPC-solidified soil," *Construction and Building Materials,* vol. 432, p. 136591, 2024/06/21/ 2024, doi: https://doi.org/10.1016/j.conbuildmat.2024.136591.
[78] W. Wang *et al.*, "Composite geopolymer based on copper tailings: Mechanical properties, strength models and microstructure," *Journal of Environmental Chemical Engineering,* vol. 13, no. 3, p. 117112, 2025/06/01/ 2025, doi: https://doi.org/10.1016/j.jece.2025.117112.
[79] S. Singh, A. Kumar, and T. G. Sitharam, "Investigating the strength and durability properties of alkali activated red mud for tailings pond embankment material," *Geomechanics for Energy and the Environment,* vol. 36, p. 100500, 2023/12/01/ 2023, doi: https://doi.org/10.1016/j.gete.2023.100500.
[80] S. E. Hosseini, A. Tabarsa, and A. Bahmanpour, "Experimental study of subgrade soil stabilised with geopolymer based on glass powder and calcium carbide," *Road Materials and Pavement Design,* vol. 24, no. 9, pp. 2209-2224, 2023.
[81] B. Shu *et al.*, "Study on laboratory and engineering application of multi source solid waste based soft soil solidification materials," *Case Studies in Construction Materials,* vol. 17, p. e01465, 2022/12/01/ 2022, doi: https://doi.org/10.1016/j.cscm.2022.e01465.
[82] S. Blotevogel *et al.*, "The influence of Al2O3, CaO, MgO and TiO2 content on the early-age reactivity of GGBS in blended cements, alkali-activated materials and supersulfated cements," *Cement and Concrete Research,* vol. 178, p. 107439, 2024/04/01/ 2024, doi: https://doi.org/10.1016/j.cemconres.2024.107439.
[83] N. A. Odeh and A. H. J. Al-Rkaby, "Strength, Durability, and Microstructures characterization of sustainable geopolymer improved clayey soil," *Case Studies in Construction Materials,* vol. 16, p. e00988, 2022/06/01/ 2022, doi: https://doi.org/10.1016/j.cscm.2022.e00988.

[84] Z. Luo *et al.*, "Experimental investigation of unconfined compression strength and microstructure characteristics of slag and fly ash-based geopolymer stabilized riverside soft soil," *Polymers,* vol. 14, no. 2, p. 307, 2022.
[85] M. Nabizadeh Mashizi, M. H. Bagheripour, M. M. Jafari, and E. Yaghoubi, "Mechanical and microstructural properties of a stabilized sand using geopolymer made of wastes and a natural pozzolan," *Sustainability,* vol. 15, no. 4, p. 2966, 2023.
[86] X. Wu *et al.*, "Behavior of hematite, magnetite, and reduced iron powder in geopolymers: Effects of mechanical properties and reaction mechanism," *Journal of Cleaner Production,* vol. 444, p. 141178, 2024.
[87] R. Obenaus-Emler, M. Falah, and M. Illikainen, "Assessment of mine tailings as precursors for alkali-activated materials for on-site applications," *Construction and Building Materials,* vol. 246, p. 118470, 2020.
[88] Z.-J. Chen, R.-D. Zhao, H.-Y. Fang, W.-B. Chen, R.-J. Zhang, and J.-H. Yin, "Effects of rates of consolidation on low-carbon solidification of marine deposits with recycled ISSA and GGBS," *Case Studies in Construction Materials,* vol. 22, p. e04722, 2025.
[89] I. A. Khasib, N. N. Nik Daud, and M. Izadifar, "Consolidation behaviour of palm-oil-fuel-ash-based geopolymer treated soil," *Geotechnical Research,* vol. 10, no. 3, pp. 138-152, 2023.
[90] M. Johnson Singh, W. Feng, D.-s. Xu, M. Dubey, and L. Borana, "Long-term elastoviscoplastic behavior of fly ash–blended Indian montmorillonite clay in oedometer conditions," *International Journal of Geomechanics,* vol. 22, no. 3, p. 04021306, 2022.
[91] A. Amiri, M. M. Toufigh, and V. Toufigh, "Stabilisation of organic soils with alkali-activated binders," *International Journal of Pavement Engineering,* vol. 24, no. 2, p. 2104844, 2023.
[92] J. Li, Y. Liu, X. Ke, X. Jiao, R. Li, and C. Shi, "Geopolymer synthesized from electrolytic manganese residue and lead-zinc smelting slag: Compressive strength and heavy metal immobilization," *Cement and Concrete Composites,* vol. 134, p. 104806, 2022/11/01/ 2022, doi: https://doi.org/10.1016/j.cemconcomp.2022.104806.
[93] C. Chen, H. Liu, Y. Zhang, G. Gu, and J. Hu, "Micro-assessment of heavy metal immobilization within alkali-activated copper tailings-slag geopolymer," *Cement and Concrete Composites,* vol. 149, p. 105510, 2024/05/01/ 2024, doi: https://doi.org/10.1016/j.cemconcomp.2024.105510.
[94] F. Pahlavan, H. Kaur, L. K. G. Ackerman-Biegasiewicz, A. Lamanna, and E. H. Fini, "Application of algal biochar to prevent leachate of heavy metals from mine tailings," *Resources, Conservation and Recycling,* vol. 210, p. 107810, 2024/11/01/ 2024, doi: https://doi.org/10.1016/j.resconrec.2024.107810.
[95] O. E. Ige, O. A. Olanrewaju, K. J. Duffy, and C. Obiora, "A review of the effectiveness of Life Cycle Assessment for gauging environmental

impacts from cement production," *Journal of Cleaner Production,* vol. 324, p. 129213, 2021/11/15/ 2021, doi: https://doi.org/10.1016/j.jclepro.2021.129213.
[96] M. Tao, D. Lu, Y. Shi, and C. Wu, "Utilization and life cycle assessment of low activity solid waste as cementitious materials: A case study of titanium slag and granulated blast furnace slag," *Science of The Total Environment,* vol. 849, p. 157797, 2022/11/25/ 2022, doi: https://doi.org/10.1016/j.scitotenv.2022.157797.
[97] R. Bajpai, K. Choudhary, A. Srivastava, K. S. Sangwan, and M. Singh, "Environmental impact assessment of fly ash and silica fume based geopolymer concrete," *Journal of Cleaner Production,* vol. 254, p. 120147, 2020/05/01/ 2020, doi: https://doi.org/10.1016/j.jclepro.2020.120147.
[98] W. Tang, G. Pignatta, and S. M. Sepasgozar, "Life-cycle assessment of fly ash and cenosphere-based geopolymer material," *Sustainability,* vol. 13, no. 20, p. 11167, 2021.
[99] E. Medina-Martos *et al.*, "Environmental and economic performance of carbon capture with sodium hydroxide," *Journal of CO2 Utilization,* vol. 60, p. 101991, 2022/06/01/ 2022, doi: https://doi.org/10.1016/j.jcou.2022.101991.
[100] B. Ali, M. H. E. Ouni, and R. Kurda, "Life cycle assessment (LCA) of precast concrete blocks utilizing ground granulated blast furnace slag," *Environmental Science and Pollution Research,* vol. 29, no. 55, pp. 83580-83595, 2022.
[101] Q. Tushar, M. A. Bhuiyan, Z. Abunada, C. Lemckert, and F. Giustozzi, "Carbon Footprint and Uncertainties of Geopolymer Concrete Production: A Comprehensive Life Cycle Assessment (LCA)," *C,* vol. 11, no. 3, p. 55, 2025.
[102] V. Zetola *et al.*, "From Mine Waste to Construction Materials: A Bibliometric Analysis of Mining Waste Recovery and Tailing Utilization in Construction," *Sustainability (2071-1050),* vol. 16, no. 23, 2024.
[103] L. R. Adrianto and S. Pfister, "Prospective environmental assessment of reprocessing and valorization alternatives for sulfidic copper tailings," *Resources, Conservation and Recycling,* vol. 186, p. 106567, 2022.
[104] H. R. Manaviparast, T. Miranda, E. Pereira, and N. Cristelo, "A comprehensive review on mine tailings as a raw material in the alkali activation process," *Applied Sciences,* vol. 14, no. 12, p. 5127, 2024.